

# Thermal axion production at hard and soft momenta

---

Killian Bouzoud,<sup>a</sup> Jacopo Ghiglieri<sup>a</sup>

<sup>a</sup>*SUBATECH, Nantes Université, IMT Atlantique, IN2P3/CNRS,  
4 rue Alfred Kastler, La Chantrerie BP 20722, 44307 Nantes, France*

*E-mail:* [killian.bouzoud@subatech.in2p3.fr](mailto:killian.bouzoud@subatech.in2p3.fr),  
[jacopo.ghiglieri@subatech.in2p3.fr](mailto:jacopo.ghiglieri@subatech.in2p3.fr)

ABSTRACT: Hot axions, thermally produced in the Early Universe, would contribute to dark radiation and are thus subject to present and future constraints from  $N_{\text{eff}}$ . In this paper we quantify the contribution to  $N_{\text{eff}}$  and its uncertainty in models with axion-gluon couplings from thermal dynamics above the QCD transition. In more detail, we determine the leading-order thermal axion production rate for axion momenta of the order of the temperature adopting three different schemes for the incorporation of the collective dynamics of soft gluons. We show how these three schemes extrapolate differently into the regime of softer axion production, thus giving us a first quantitative handle on the theory uncertainty of the rate. Upon solving the Boltzmann equation, we find that this theory uncertainty translates to an uncertainty of order 0.002 for the contribution to  $N_{\text{eff}}$  prior to the QCD crossover. The uncertainty from common momentum-averaged approximations to the Boltzmann equation is smaller. We also discuss how QCD transition dynamics would need to be integrated into our results and we show how existing rate determinations in the literature based on gauge-dependent resummations are problematic.

---

## Contents

<b>1</b>	<b>Introduction</b>	<b>1</b>
<b>2</b>	<b>Collective effects, scale separation and Hard Thermal Loop resummation</b>	<b>3</b>
2.1	The naive approach to the rate and the emergence of collective effects	4
2.2	Collective effects and resummation in the literature	7
2.3	Novel LO-accurate schemes	9
<b>3</b>	<b>Numerical results for the production rate</b>	<b>13</b>
<b>4</b>	<b>Momentum-dependent axion freeze-out above the QCD crossover</b>	<b>18</b>
<b>5</b>	<b>Conclusions</b>	<b>24</b>
<b>A</b>	<b>Phase-space integrations</b>	<b>27</b>
<b>B</b>	<b>Gauge-dependent resummations in the literature</b>	<b>32</b>
<b>C</b>	<b>Theory uncertainty in perturbative thermal QCD</b>	<b>40</b>

---

## 1 Introduction

The axion was introduced in [1–3] as a simple, elegant solution to the so-called strong CP problem of Quantum Chromodynamics (QCD). It was later realized in [4–6] that such a new field could account for the observed amount of dark matter — see [7, 8] for reviews. Here we rather focus on another cosmological consequence: the couplings between the axion and the Standard Model (SM) particles cause *thermal production* of *hot axions* during the radiation epoch of the early universe.

In a nutshell, for temperatures  $T$  sufficiently lower than the axion scale  $f_{\text{PQ}}$ ,<sup>1</sup> axion-SM interactions are encoded by non-renormalizable operators suppressed by powers of  $T/f_{\text{PQ}}$ . Hence, at sufficiently high temperatures ultrarelativistic axions will be in equilibrium with the other bath constituents, to later *freeze out*. This frozen-out abundance constitutes *dark radiation* and is thus constrained by the number  $N_{\text{eff}}$  of light degrees of freedom at the epochs of Big Bang Nucleosynthesis (BBN) and of Cosmic Microwave Background (CMB) decoupling. Therefore, determinations of the frozen-out abundance can be used, together with observational constraints, to probe parameters of axion modes, chiefly  $f_{\text{PQ}}$  itself. We mention

---

<sup>1</sup>We use this somewhat nonstandard notation, where PQ stands for Peccei–Quinn, rather than the more common  $f_a$ , because later on we shall reserve that symbol for the axion phase-space distribution.

that Planck data [9] yield  $N_{\text{eff}} = 2.99 \pm 0.17$  and combined BBN data give  $N_{\text{eff}} = 2.898 \pm 0.141$  [10], from which any particle degree of freedom having frozen out around or after the QCD crossover transition at  $T_c \approx 150$  MeV can already be excluded.

These observational limits are expected to improve by an order of magnitude with future detectors [11–13], making higher freeze-out temperatures accessible and approaching the uncertainty of existing high-precision theory determinations of  $N_{\text{eff}}$  in the SM [14–17]. This then motivates a renewed look at calculations of the interaction rate of axions in the early universe, which is the key ingredient for the determination of the frozen-out abundance. It is defined as

$$\partial_t f_a(k) - Hk \partial_k f_a(k) = \Gamma(k) [n_{\text{B}}(k) - f_a(k)], \quad (1.1)$$

where  $f_a(k) \equiv (2\pi)^3 dN_a / (d^3\mathbf{k} d^3\mathbf{x})$  is the axion phase-space density and  $n_{\text{B}}(k) \equiv (\exp(k/T) - 1)^{-1}$  its Bose–Einstein form in equilibrium. As the axion mass is negligible for hot axions,  $E_k \approx k$ , where  $k \equiv |\mathbf{k}|$  is the modulus of their three-momentum.  $H$  is the Hubble rate. As the axion production rate  $\Gamma(k)$  depends on the momentum, the notion of a freeze-out temperature is meaningful only when axion decoupling is fast enough that all modes freeze out in a narrow temperature range, well approximated by a single one. This was already discussed in [18, 19]: we will address this issue quantitatively and discuss similarities with the recent analysis in [20].

Our main goal, however, is the precise determination of  $\Gamma(k)$  itself. We will concentrate on the KSVZ model [21, 22] where the axion can only interact with gluons. Calculations of  $\Gamma(k)$  have a long history, starting from [23, 24], leading to the existing perturbative determinations and phenomenological consequences in [25–29]. As we shall illustrate, gluon-mediated processes are very sensitive to the collective effects of a QCD plasma, which perturbatively first appear at momenta (wavelengths) smaller (larger) than  $g_3 T$  ( $1/g_3 T$ ), where  $g_3$  is the QCD gauge coupling. These collective effects cure would-be infrared (IR) divergences of the rate; their implementation requires resummed propagators and vertices, such as those arising from the Hard Thermal Loop (HTL) effective theory [30, 31]. As the separation between the *soft scale*  $g_3 T$  and the *hard scale* defined by the temperature becomes blurred once  $T$  approaches  $T_c$ , the reliability of these perturbative calculations can be called into question, see [18, 19].

Here we shall discuss in detail the physics responsible for the soft-gluon contribution to  $\Gamma(k)$  and explain how it is dealt with in existing calculations. We shall also explain how these calculations become *extrapolations* once *soft axion momenta*,  $k \lesssim g_3 T$ , are considered, giving rise to issues of negativity and gauge dependence. We shall then introduce two prescriptions which are novel in the context of axion production, inspired respectively by previous work on right-handed-neutrino and gravitational-wave production [32–34] and by QCD kinetic theory implementations [35]. We shall show how both are gauge invariant and how the latter in particular stays positive definite by construction under extrapolation to  $k \lesssim g_3 T$ . We shall also discuss the pathologies that arise from the gauge-dependent resummation method of [26, 36].

Following methods in use in the hot QCD literature — see App. C — we will be able to give a first estimate of the uncertainty of the rate by comparing our determinations and previous ones. We will show how this uncertainty translates quantitatively on the freeze-out mechanism and the resulting abundance. As we mention, we shall also quantify the uncertainty related to adopting momentum-integrated approximations as opposed to our momentum-dependent implementation of Eq. (1.1).

The paper is organized as follows: in Sec. 2 we present a pedagogical introduction to the emergence of collective effects in calculations of axion production, showing how they are incorporated, with their limitations. We then introduce our prescriptions. In Sec. 3 we present numerical results for the rate resulting from the new prescriptions and compare them with existing determinations, paving the way for Sec. 4. There, we insert these rates in the Boltzmann equation (1.1) and present our solutions with full accounting of momentum dependence. We then proceed to quantify the uncertainties stemming from the rate and those arising from the momentum-averaged approximations. Finally, in Sec. 5 we draw our conclusions. Details on the technical implementation of the rates and on the comparison with the literature are to be found in the appendices, together with a brief summary of hot QCD methods and results for the assessment of the theory uncertainty of perturbative calculations.

## 2 Collective effects, scale separation and Hard Thermal Loop resummation

Let us start by briefly discussing the mechanisms that may keep hot axions in thermal equilibrium at some early point in the thermal history of the universe. At energies well below the axion scale  $f_{\text{PQ}}$ , the most generic axion-SM effective Lagrangian reads — see e.g. [26]

$$\begin{aligned} \mathcal{L} = & \mathcal{L}_{\text{SM}} + \frac{1}{2}(\partial_\mu a)(\partial^\mu a) - \frac{a}{f_{\text{PQ}}} \left[ c_3 \frac{\alpha_3}{8\pi} G_{\mu\nu}^b \tilde{G}^{\mu\nu} + c_2 \frac{\alpha_2}{8\pi} W_{\mu\nu}^j \tilde{W}^{\mu\nu} + c_1 \frac{\alpha_1}{8\pi} B_{\mu\nu} \tilde{B}^{\mu\nu} \right] \\ & + i c_t y_t \frac{a}{f_{\text{PQ}}} \bar{Q}_L \sigma_2 H^* u_R + \text{h.c.}, \end{aligned} \quad (2.1)$$

where  $a$  is the axion field,  $\alpha_i = g_i^2/4\pi$  with the  $g_i$  being the coupling constants of the different gauge groups and  $\tilde{T}^{\mu\nu} = 1/2\varepsilon^{\mu\nu\rho\sigma}T_{\rho\sigma}$  is the dual of the tensor  $T$ , with  $G$ ,  $W$  and  $B$  the SU(3), SU(2) and U(1) field-strength tensors. h.c. denotes the Hermitean conjugate,  $\sigma_2$  is a Pauli matrix and  $y_t$  is the top Yukawa coupling,. All other SM Yukawa couplings can be considered negligible.

The specificities of each axion model are encoded in the various  $c$  Wilson coefficients. As we mentioned, here we focus on thermal axion production in the KSVZ model [21, 22], where the axion can only interact with gluons, implying  $c_1 = c_2 = c_t = 0$  and  $c_3 = 1$ . In this model the only processes for producing one axion are, at leading order (LO) in the coupling  $g_3$ , the  $2 \leftrightarrow 2$  ones in Figure 1. There is just one free parameter, that is the axion scale  $f_{\text{PQ}}$ . This model is therefore an ideal testing ground for the exploration of the reliability of perturbative determinations of the rate and it is at the same time of high phenomenological interest. According to the analysis of [27, 28], values of  $f_{\text{PQ}}$  close to the lower bound resulting

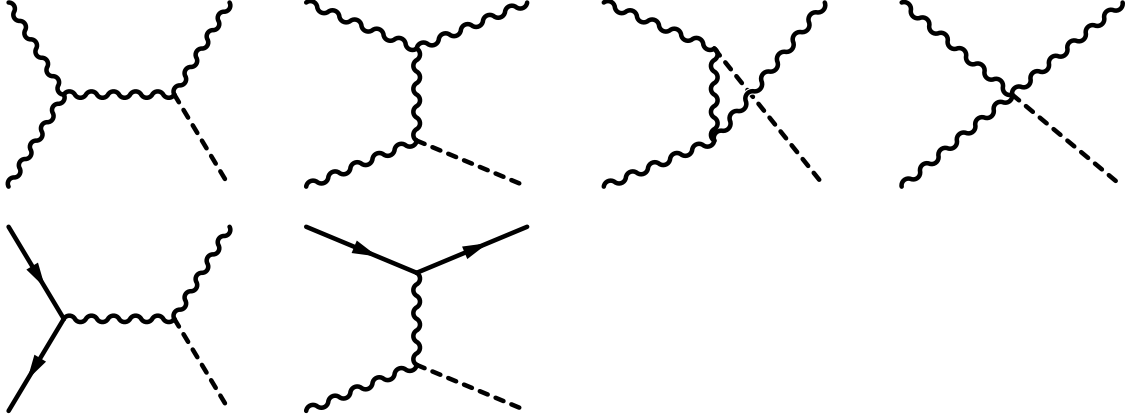


**Figure 1:**  $1+2 \rightarrow 3+a$  processes in the KSVZ model. Wiggly lines represent gluons, arrowed lines represent fermions and dashed lines represent axions.

from astrophysical constraints could give a  $\Delta N_{\text{eff}}$  contribution that would be accessible to the next-generation CMB telescopes.

In the remainder of this Section we first discuss the naive Boltzmann-equation approach to axion production, its limitations and the emergence of collective effects in Sec. 2.1; this subsection is rather pedagogical, expert readers can skip to Sec. 2.2, where we discuss the implementation of collective effects in the literature. Finally, in Sec. 2.3 we introduce our resummation schemes. Numerical results are presented in the following Section. A similar analysis has been recently presented in [37] for freeze-in dark matter production.

## 2.1 The naive approach to the rate and the emergence of collective effects

Let us now discuss the determination of the rate  $\Gamma(k)$ . Naive kinetic theory and the Boltzmann equation give

$$\Gamma(k)^{\text{naive}} = \frac{1}{4k} \int d\Omega_{2 \leftrightarrow 2} \sum_{1,2,3 \in \text{SM}} |\mathcal{M}_{1+2 \rightarrow 3+a}|^2 \frac{f_1(p_1) f_2(p_2) [1 \pm f_3(k_1)]}{n_B(k)}, \quad (2.2)$$

where considerations on the validity region of this approach will be presented soon. The equilibrium phase-space distributions are  $f_i(p) = n_B(p)$  when  $i$  is bosonic and conversely  $f_i(p) = n_F(p) \equiv (\exp(p/T) + 1)^{-1}$  when fermionic.  $p_1, p_2, k_1, k$  are the momenta of the two incoming particles 1, 2 and of the outgoing 3 and  $a$  respectively, and the  $1 + n_B$  or  $1 - n_F$  accounts for final-state Bose enhancement and Pauli blocking. The factor of  $1/4k$  corresponds to a standard  $1/2k$  Lorentz-invariant phase space multiplying a factor of  $1/2$  to account for identical particles in the initial state and to neutralize double-counting in the sums when particles 1 and 2 are different.

The final ingredient in (2.2) are the matrix elements squared  $|\mathcal{M}_{1+2 \rightarrow 3+a}|^2$ , summed over all degeneracies of particles 1, 2, 3. These are to be integrated over the  $2 \leftrightarrow 2$  phase space  $d\Omega_{2 \leftrightarrow 2}$ , as given by Eq. (A.1) in App. A. We obtained said matrix elements using automated

techniques. The basic workflow we followed was as such, as in [34]: first obtain the Feynman rules using FEYNRULES [38], then call FEYNARTS [39] to generate all possible processes and finally use FORMCALC [40] to compute the amplitudes associated with each process and square them. The Lagrangian implemented in the model file for FEYNRULES was Eq. (2.1) with the Wilson coefficients later set to the values of the KSVZ model. Our results agree with those of [25] and read

$$|\mathcal{M}_{g+g\rightarrow g+a}|^2 = \frac{g_3^6(N_c^2 - 1)N_c}{32\pi^4 f_{\text{PQ}}^2} \left[ \frac{su}{t} + \frac{st}{u} + \frac{tu}{s} \right], \quad |\mathcal{M}_{q+g\rightarrow q+a}|^2 = -\frac{g_3^6 C_F N_c}{64\pi^4 f_{\text{PQ}}^2} \frac{s^2 + u^2}{t}, \quad (2.3)$$

where the quark is taken to be a Dirac quark of negligible mass and the  $q\bar{q} \rightarrow ga$  can be obtained by crossing.  $C_F = (N_c^2 - 1)T_F/(N_c)$  is the quadratic Casimir of the fundamental representation of  $\text{SU}(N_c = 3)$  and  $T_F = 1/2$ .  $s$ ,  $t$  and  $u$  are the usual Mandelstam invariants,  $s \equiv (P_1 + P_2)^2$ ,  $t \equiv (P_1 - K_1)^2$ , with on-shell external momenta  $P_i = (p_i, \mathbf{p}_i)$ . We denote four-momenta by capital letters, moduli of three-momenta by lowercase ones. Our metric is the mostly-minus one.

Hence, one can see that Eq. (2.2) is predicated on the assumption of the existence of on-shell massless particles in the thermal plasma of the early universe. In a thermal QCD plasma, particle states that are massless in vacuum develop *thermal masses* of the order of  $g_3 T$  [41–43].<sup>2</sup> These however are not important at LO for the external states, as the phase-space integral is dominated by regions where the external states have momenta of  $\mathcal{O}(T)$ .

The second so-far unstated assumption undergirding Eq. (2.2) can be made explicit by plugging in Eq. (2.2) the matrix elements in Eq. (2.3). We find

$$\Gamma(k)_{\text{KSVZ}}^{\text{naive}} = \frac{g_3^6(N_c^2 - 1)}{128\pi^4 f_{\text{PQ}}^2 k} \int d\Omega_{2\leftrightarrow 2} \left\{ N_c \left[ 2\frac{su}{t} + \frac{tu}{s} \right] \frac{n_{\text{B}}(p_1)n_{\text{B}}(p_2)[1 + n_{\text{B}}(k_1)]}{n_{\text{B}}(k)} \right. \\ \left. - 2T_F N_f \frac{s^2 + u^2}{t} \frac{n_{\text{F}}(p_1)n_{\text{B}}(p_2)[1 - n_{\text{F}}(k_1)]}{n_{\text{B}}(k)} \right. \\ \left. + T_F N_f \frac{t^2 + u^2}{s} \frac{n_{\text{F}}(p_1)n_{\text{F}}(p_2)[1 + n_{\text{B}}(k_1)]}{n_{\text{B}}(k)} \right\}, \quad (2.4)$$

where  $N_f$  denotes the number of quark flavors that can be considered light. We shall return to this in Sec. 3. We have further used a relabeling of  $P_1$  into  $P_2$  and vice-versa to shuffle the  $u$  denominators into  $t$  ones on the first and second line. These  $t$  denominators are precisely linked to the assumption we need to make explicit: when integrating over the phase space, these denominators are responsible for would-be IR divergences. These  $t$  denominators are best integrated using the  $t$ -channel parametrization detailed in Eq. (A.2) in App. A, which keeps as explicit integration variables the frequency and momentum exchange  $q^0$  and  $q$ , the momentum  $p_1$  and an azimuthal angle  $\phi$ , with  $P_2 = K - Q$ .  $t$  then becomes  $t = q_0^2 - q^2$ . At

---

<sup>2</sup>This is true in a very broad class of quantum field theories, including gauge theories, where the mass is of the order of the gauge coupling  $g$  times the temperature. Here we concentrate for simplicity on the QCD sector of the SM due to its direct coupling to axions in our chosen model.

small  $t$  we can then find the would-be divergent contribution from a  $t \ll s \sim T$  expansion, finding

$$\Gamma(k)_{\text{KSVZ}}^{\text{naive div}} = \frac{g_3^6(N_c^2 - 1)}{2^{13}\pi^7 f_{\text{PQ}}^2 k^2} \int_{q \ll k} dq \int_{-q}^q dq_0 \int_0^\infty dp_1 \int_{-\pi}^\pi \frac{d\varphi}{2\pi} \\ \times \left\{ -2N_c \frac{s^2}{t} n_{\text{B}}(p_1)[1 + n_{\text{B}}(p_1)] - 4T_F N_f \frac{s^2}{t} n_{\text{F}}(p_1)[1 - n_{\text{F}}(p_1)] \right\}. \quad (2.5)$$

The expression for  $s$  in Eq. (A.3) can be used to simplify the matrix element squared into

$$\frac{s^2}{t} \stackrel{k, p_1 \gg Q}{\approx} \frac{4k^2 p_1^2 (q_0^2 - q^2)(1 - \cos \varphi)^2}{q^4}. \quad (2.6)$$

Plugging this in Eq. (2.5) and performing the  $p_1$  and  $\varphi$  integrations leads to

$$\Gamma(k)_{\text{KSVZ}}^{\text{naive div}} = \frac{g_3^6(N_c^2 - 1)T^3}{2^{11}\pi^5 f_{\text{PQ}}^2} \int_{q \ll k} dq \int_{-q}^q dq_0 \frac{(q^2 - q_0^2)}{q^4} \left\{ N_c + T_F N_f \right\} \\ = \frac{g_3^4(N_c^2 - 1)T m_{\text{D}}^2}{2^9 \pi^5 f_{\text{PQ}}^2} \int_{q \ll k} \frac{dq}{q}, \quad (2.7)$$

where we have noted that the first line is proportional to the QCD *Debye mass*, which reads at LO

$$m_{\text{D}}^2 = \frac{g_3^2 T^2}{3} (N_c + T_F N_f). \quad (2.8)$$

This quantity is the so-called chromoelectric screening mass: it is of order  $g_3 T$  and it marks the first appearance of collective excitations, which screen long-wavelength electrostatic gluons. In our case it multiplies the would-be IR divergence  $dq/q$ ; as soon as  $q \sim g_3 T$  our naive description in terms of bare, in-vacuum matrix elements breaks down, precisely because it cannot, by construction, capture collective effects arising at that scale. This is precisely the second unstated assumption: the naive approach is only valid when  $Q \gg g_3 T$ .

In our specific case, the naive approach misses *Landau damping*, sometimes also called *dynamical screening* [44, 45]. This collective effect ends up shielding the would-be divergence thanks to the emergence not just of a screening mass but also of a width for space-like soft gluons, corresponding to their damping rate. Proper accounting of this phenomenon requires then abandoning, at least for the  $Q \sim g_3 T$ ,  $K \sim P_1 \sim T$  region, the naive approach based on bare matrix elements and replacing it with some form of resummation encoding these collective effects.

This is of course not new. Indeed, shortly after the development of the Hard Thermal Loop effective theory [30, 31], which describes in a gauge-invariant manner these collective excitations through resummed propagators and vertices, [23] applied HTL resummation to the abelian version of the problem at hand. In the next Subsection we explain in more detail this and other implementations of resummation in the literature and introduce ours.

We conclude this Subsection by noting one final limitation of the naive approach: it also requires the axion to be hard, with momentum obeying  $k \gg g_3 T$ . For  $k \lesssim g_3 T$  one can on

the other hand expect collective effects to play an important, LO role, leading again to a breakdown of Eq. (2.2). Properly dealing with this region requires more intricate approaches than the relatively simple resummations presented in the next Subsections; indeed, there currently exist no calculation of thermal production rates for light particles that are valid in the  $k \sim g_3 T$  regime, neither in the context of early-universe cosmology — see [32, 34] for ultrarelativistic right-handed neutrinos and gravitational waves — or in hot QCD — see [46–48]. We will return later to this, when discussing extrapolating to this regime.

## 2.2 Collective effects and resummation in the literature

As we mentioned, Landau damping was first introduced to the context of the axion production rate in [23] for the abelian case.<sup>3</sup> It can be accounted for by applying Thermal Field Theory (TFT) and HTL resummation. The former yields the well-known relation

$$\Gamma(k) = \frac{1}{k} \text{Im} \Pi_a^R(k, k), \quad (2.9)$$

where  $\Pi_a^R(k, k)$  is the retarded axion self-energy evaluated on the light cone, i.e. [49]

$$\Pi_a^R(K) = \int d^4 X e^{iK \cdot X} \theta(x^0) \langle [J(X), J(0)] \rangle, \quad \text{where } J \stackrel{\text{KSVZ}}{=} \frac{\alpha_3}{8\pi f_{\text{PQ}}} G_{\mu\nu}^b \tilde{G}_b^{\mu\nu}. \quad (2.10)$$

In arbitrary models  $J$  is the operator coupling to the axion field,  $\mathcal{L} \supset -aJ$ . With the methods of [49] one can show that Eq. (2.9) is correct to first order in the axion-SM couplings and to all orders in the internal SM couplings.

In the approach of [23] one can then use Eq. (2.4) up to an IR cutoff  $q^*$  on the  $dq$  integration. This cutoff must be chosen such that  $g_3 T \ll q^* \ll T$ , so that HTL resummation can be performed only for  $q \ll q^*$ . There one can use Eq. (2.9). Evaluating Eq. (2.10) one encounters at LO for  $k \gtrsim T$  and soft  $Q$  the diagram on the left of Fig. 2, where the lower gluon line carries the loop momentum  $Q \sim g_3 T$ , while the upper line carries  $K - Q \approx K \gtrsim T$ . Hence it is only the lower line that needs HTL resummation, whereas the upper one can be kept in its bare form. An identical contribution comes from the diagram where the upper gluon is soft and lower one hard.

We recall that HTLs are the infrared, gauge-invariant limits of one-loop thermal amplitudes with hard loop momentum  $P \sim T$  and soft external momenta  $Q_i \sim g_3 T$ . HTL resummation accounts for the emergence of collective effects at that scale. We also note that the imaginary part of the diagram on the left in Fig. 2 is given by its cut; the cut upper bare gluon is proportional to  $\delta((K - Q)^2) \approx \delta(2Q \cdot K)$ , which forces  $Q$  to be space-like in the  $K \gg Q$  limit. This in turn makes the cut HTL gluon Landau-damped. Hence, the cut of this diagram corresponds to the square of the diagram shown on the right of Fig. 2 and its counterpart with external quarks or antiquarks replacing the incoming and outgoing gluons at the top.

---

<sup>3</sup>This approach is based on HTL resummation. As the photon and gluon HTL propagators differ only in the respective Debye masses, nothing changes qualitatively in the non-abelian case at leading order.



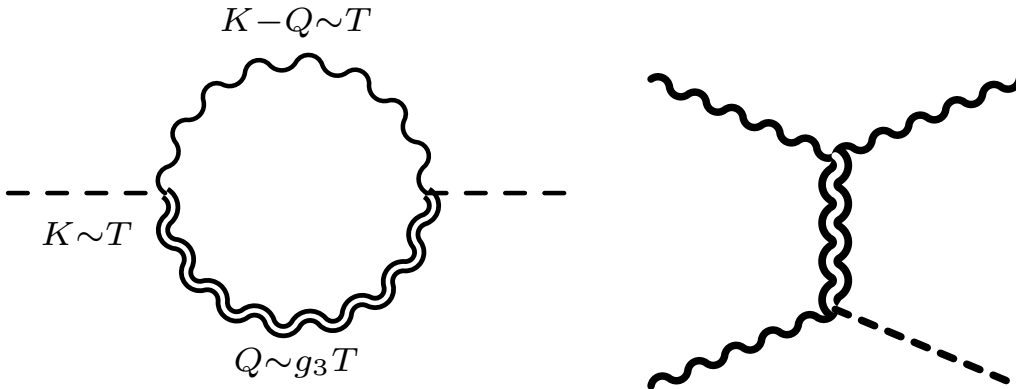


**Figure 2:** Left: one-loop axion self-energy. The upper wiggly line denotes a bare gluon with a hard thermal momentum, while the double wiggly line stands for a soft, HTL-resummed gluon. Cutting this one-loop axion self-energy corresponds to the square of the diagram on the right. We don’t show its analogue with a quark or antiquark external scatterer replacing the top ingoing and outgoing gluons.

The HTL-resummed result then yields [23]

$$\Gamma(k)_{\text{KSVZ}}^{\text{HTL [23]}} = \frac{g_3^4(N_c^2 - 1)T}{2^{10}\pi^6 f_{\text{PQ}}^2} \int_0^{q^*} dq q^3 \int_{-q}^q \frac{dq^0}{q^0} \left(1 - \frac{q_0^2}{q^2}\right) \left[\rho_L(Q) + \left(1 - \frac{q_0^2}{q^2}\right) \rho_T(Q)\right], \quad (2.11)$$

where  $\rho_L$  and  $\rho_T$  are the longitudinal and transverse HTL spectral function, obtained from the retarded propagators in Eqs. (A.31)-(A.32) from  $\rho \equiv G_R - G_A$ . We remark that, up to the overall prefactor, Eq. (2.11) agrees with the leading-order soft contribution to the “transverse momentum broadening coefficient”  $\hat{q}$  in QCD plasmas — see for instance Eqs. (36) and (59) in [50]. We shall make use of this later.

One can easily check from the UV limit  $q \sim q^* \gg g_3 T$  of the spectral functions, i.e.

$$\rho_L(Q) \rightarrow \frac{\pi m_{\text{D}}^2 q^0}{q^5}, \quad \rho_T(Q) \rightarrow -\frac{\pi m_{\text{D}}^2 q^0}{2q^3 Q^2}, \quad (2.12)$$

that Eq. (2.11) contains a UV logarithmic divergence in  $q^*$  that cancels the opposite IR one of the bare, naive contribution. Hence, summing the two gives rise to a finite, regulator-independent contribution. This is the approach that has been implemented for the KSVZ model in [25],<sup>4</sup> i.e.

$$\Gamma(k)_{\text{KSVZ}}^{\text{strict LO [25]}} = \Gamma(k)_{\text{KSVZ}}^{\text{naive}} \Big|_{q>q^*} + \Gamma(k)_{\text{KSVZ}}^{\text{HTL [23]}} \quad (2.13)$$

This implementation is a *strict LO scheme* for hard axions with  $k \gtrsim T$ : it does not resum any partial subset of higher order effects — HTL resummation in the  $Q \ll K \gtrsim T$  range is

<sup>4</sup>The earlier implementation in [24] cut off the IR divergence with the Debye mass and is thus only valid at leading-logarithmic accuracy.

a strict LO effect. The resulting function of momentum contains a  $\ln(k/m_D)$  term, which clearly highlights the validity region of the calculation: when *extrapolating* to  $k < m_D$  this term becomes negative and for  $k \ll m_D$  it turns the entire rate negative. This is easily seen in Fig. 3, where the dotted green curve becomes negative at small  $k$ . As the temperature decreases the QCD coupling increases and the scale separation between  $k \gtrsim T$  and  $m_D$  becomes blurry, making the  $k$  range with negative unphysical rates larger. This is a common feature to calculations adopting the strict LO scheme defined by the method of [23] — see the detailed analysis in [51] for the analogous case of thermal axino production.

As explained there, the optimal way to proceed would be to carry out a calculation in the  $k \sim g_3 T$  regime. However, as we have mentioned, no such calculation has been performed in the literature for any production rate of light-like particles. Here we do not present such an ambitious calculation; rather, we introduce to the context of axion production two different schemes for the axion rate for  $k \gtrsim T$  that extrapolate better to the  $k \lesssim m_D$  regime. This is presented in the next subsection.

We conclude by commenting on another approach in the literature [26], based on a gauge-dependent resummation first introduced for gravitinos in [36]. It relies on the idea of using the full, rather than HTL, gluon spectral functions at one loop in Feynman gauge, thus avoiding the need of separating the soft, HTL resummed region from the hard, bare one and giving rise to a positive-definite integrand and rate. While this might sound like a sound and sensible approach, it is well known, starting from [52, 53], that the full one-loop transverse spectral function contains a gauge-dependent double-pole divergence for  $q^0 \approx 0$ ,  $q \sim g_3^2 T$ , signaling the emergence of an unphysical sensitivity to the chromomagnetic scale where perturbation theory breaks down [54]. [55] carried out a similar analysis for momentum broadening in QCD plasmas and concluded that resumming full self-energies for all  $Q$  in Feynman gauge — or any other gauge — gives rise to the same pathological divergence. As the soft contribution to transverse momentum broadening is, up to prefactors, the same as in Eq. (2.11), their conclusions apply to this case as well. We shall return to this later in the main text. We will also prove the emergence of this extra unphysical divergence in great detail in App. B.

### 2.3 Novel LO-accurate schemes

In this section we shall exploit the freedom to resum subsets of higher-order terms in the  $k \gtrsim T$  LO rate to define two new *schemes* that are equivalent to the strict LO one at vanishing coupling. This is a commonplace technique in hot QCD, where it has been used to study the intrinsic theory uncertainty of the perturbative expansion — see App. C for a brief overview.

Our first scheme is a slight rework of the strict LO; it was introduced for right-handed-neutrino production in [32, 33] and for gravitational-wave production in [34]. In a nutshell, one subtracts the divergent part found in Eq. (2.7) from the naive rate, leading to the finite

expression

$$\Gamma(k)_{\text{KSVZ}}^{\text{naive subtr}} = \Gamma(k)_{\text{KSVZ}}^{\text{naive}} - \frac{3g_3^4(N_c^2 - 1)Tm_D^2}{2^{11}\pi^5 f_{\text{PQ}}^2} \int_{-\infty}^k dq_0 \int_{|q^0|}^{2k-q^0} dq \frac{(q^2 - q_0^2)}{q^4}, \quad (2.14)$$

As we show in detail in App. A, we use the methods of [32] to carry out all integrals except the  $q_0$  and  $q$  analytically in  $\Gamma(k)_{\text{KSVZ}}^{\text{naive}}$ , finding a finite expression after the subtraction above. Note that we have kept the original integration limits for these variables, see Eq. (A.2). To complement Eq. (2.14) with the necessary HTL resummation we slightly change Eq. (2.11) into

$$\Gamma(k)_{\text{KSVZ}}^{\text{HTL [33, 34]}} = \frac{g_3^4(N_c^2 - 1)T}{2^{10}\pi^6 f_{\text{PQ}}^2} \int_{-\infty}^k dq_0 \int_{|q^0|}^{2k-q^0} dq \frac{q^3}{q^0} \left(1 - \frac{q_0^2}{q^2}\right) \left[\rho_L(Q) + \left(1 - \frac{q_0^2}{q^2}\right) \rho_T(Q)\right], \quad (2.15)$$

where we have kept the same integration limits of Eq. (2.14): since the UV limit of Eq. (2.15) is subtracted there, this is now necessary. As per [33, 34] we can now change variables from  $q$  to  $q_\perp \equiv \sqrt{q^2 - q_0^2}$ .<sup>5</sup> Up to order- $g_3^2$  effects we can then simplify the integration region as

$$\begin{aligned} \Gamma(k)_{\text{KSVZ}}^{\text{HTL [33, 34]}} &= \frac{g_3^4(N_c^2 - 1)T}{2^{10}\pi^6 f_{\text{PQ}}^2} \int_{-\infty}^{\infty} dq_0 \int_0^{2k} dq_\perp q_\perp \frac{q_\perp^2}{q_0^2} \left[\rho_L(Q) + \frac{q_\perp^2}{q^2} \rho_T(Q)\right] \\ &= \frac{g_3^4(N_c^2 - 1)T}{2^9\pi^5 f_{\text{PQ}}^2} \int_0^{2k} dq_\perp q_\perp^3 \left[\frac{1}{q_\perp^2} - \frac{1}{q_\perp^2 + m_D^2}\right] \\ &= \frac{g_3^4(N_c^2 - 1)Tm_D^2}{2^{10}\pi^5 f_{\text{PQ}}^2} \ln\left(1 + \frac{4k^2}{m_D^2}\right), \end{aligned} \quad (2.16)$$

where in going from the first to the second-line we used a sum rule derived for  $\hat{q}$  in [56, 57] — see also [50, 58] for more pedagogical illustrations. Adding together Eqs. (2.14) and (2.16) we then arrive at the definition of the *subtraction scheme*, namely

$$\Gamma(k)_{\text{KSVZ}}^{\text{subtr}} = \Gamma(k)_{\text{KSVZ}}^{\text{naive subtr}} + \Gamma(k)_{\text{KSVZ}}^{\text{HTL [33, 34]}}. \quad (2.17)$$

We refer to Eq. (A.17) for details on our implementation. It is important to note that  $\Gamma(k)_{\text{KSVZ}}^{\text{subtr}}$ , as it is obtained from a simple rework of the gauge-invariant strict LO scheme, is gauge invariant. Furthermore,  $\Gamma(k)_{\text{KSVZ}}^{\text{subtr}}$  is no longer a strict LO scheme: indeed, Eq. (2.16) contains higher-order terms for  $k \gtrsim T$ , where  $\ln(1 + 4k^2/m_D^2) = \ln(4k^2/m_D^2) + m_D^2/(4k^2) + \dots$ . Hence, these resummed terms start at relative order  $g_3^2$ . We have furthermore checked that, upon replacing  $\ln(1 + 4k^2/m_D^2)$  with  $\ln(4k^2/m_D^2)$  we find agreement with the strict LO results of [25], obtained by numerically integrating their expressions. Incidentally, we remark that our implementation of the strict LO rate, as per Eq. (A.18), converges faster.

It is worth noting that  $\ln(1 + 4k^2/m_D^2)$  is better behaved than  $\ln(4k^2/m_D^2)$  when *extrapolating* to  $k \ll m_D$ , as it becomes small and positive rather than large and negative. However,

---

<sup>5</sup>This  $q_\perp$  corresponds to the component of  $\mathbf{q}$  orthogonal to  $\mathbf{k}$  only at zeroth order in the  $q \ll k$  expansion. In general one has  $q_\perp^2 = (q^2 - q_0^2)((2k - q^0)^2 - q^2)/(4k^2)$ .

as Fig. 3 makes clear — compare the dotted green line with the dashed blue one — this subtraction scheme is still not positive definite at all  $k$ . This can be understood from having subtracted the divergent infrared part in the bare limit in Eq. (2.14) and having replaced it with its resummed version in Eq. (2.16). The latter, though positive definite, is smaller, thus opening the door to negativity outside of the validity region of this approach.

It is for this reason that we now introduce a positive-definite scheme. One possibility would be to follow the method introduced in [59, 60] for the effective kinetic theory of QCD. The authors exploited the liberty of defining rates that are equivalent to the strict LO at vanishing coupling but that differ by higher-order terms. In detail, they singled out divergent channels/diagrams and replaced the bare propagators therein with resummed, retarded HTL ones. In our case, we would need to do so in the second and third diagram on the first line in Fig. 1 and in the second diagram on the second line. Upon taking the square modulus of the amplitudes, as in Eq. (2.2), one naturally has a positive-definite quantity for all  $k$ . This approach would have the drawback of requiring more intricate numerical integrations over the HTL propagators. The availability in the past decade of analytical results for the soft region, as in Eq. (2.16), allows for the introduction of a numerically simpler scheme, first devised in [35] for the numerical implementation of the kinetic theory in [59]. Namely, we define our *tuned mass scheme* as

$$\Gamma(k)_{\text{KSVZ}}^{\text{tuned}} = \Gamma(k)_{\text{KSVZ}}^{\text{naive}} \quad \text{with} \quad \frac{s^2 + u^2}{t} \rightarrow \frac{q^4}{2(q^2 + \xi^2 m_{\text{D}}^2)^2} \frac{(s-u)^2}{t} + \frac{t}{2}$$

$$\text{and} \quad 2\frac{su}{t} \rightarrow -\frac{q^4}{2(q^2 + \xi^2 m_{\text{D}}^2)^2} \frac{(s-u)^2}{t} + \frac{t}{2}, \quad (2.18)$$

where  $\xi > 0$  is an  $\mathcal{O}(1)$  constant that must be *tuned* so that this method reproduces the analytical result given by Eq. (2.16) in the soft region for  $g_3 \ll 1$  and  $k \gtrsim T$ . In App. A we give the full expression for  $\Gamma(k)_{\text{KSVZ}}^{\text{tuned}}$  in Eq. (A.20) and we show explicitly that<sup>6</sup>

$$\xi = \frac{e^{1/3}}{2}. \quad (2.19)$$

This scheme too is gauge invariant, as it is obtained by suitably modifying the  $t$ -channel denominators of gauge-independent matrix elements. Furthermore, as Eq. (2.18) makes clear, for  $q \gg m_{\text{D}}$  this scheme resums higher-order effects thanks to the denominator  $(q^2 + \xi^2 m_{\text{D}}^2)^2$ . The energy dependence of the statistical factors for incoming and outgoing particle states is left unchanged, differently from what happens in the soft region of the strict LO and subtraction schemes — see Eq. (2.5). Hence this schemes does not assume  $T \gg m_{\text{D}}$ , even though it reduces to the value obtained there. We also remark that, differently from what one would naively expect from the expansion of  $q^4/(q^2 + \xi^2 m_{\text{D}}^2)^2$  for  $q \sim T \gg m_{\text{D}}$ , the difference between the strict LO scheme and this one is not of order  $g_3^2$  but rather of order  $g_3$  when  $k \gtrsim T$ . This  $\mathcal{O}(g_3)$  difference arises from the region where  $Q \sim g_3 T$  and  $p_1$  is a gluon's

---

<sup>6</sup>This scheme was recently applied in [61] to the transverse momentum broadening coefficient of QCD. Our result for  $\xi$  agrees with theirs.

momentum with  $p_1 \sim g_3 T$ , see [62–64] for analogous cases. This  $\mathcal{O}(g_3)$  deviation emerges clearly from Fig. 4, as we shall show in the next section. We shall return to the topic of  $\mathcal{O}(g_3)$  corrections later.

Compared with the strict LO and subtraction schemes, the current one has a drawback, namely that the dependence on the Debye mass is not factored out in an analytical part such as Eq. (2.16), which is readily evaluated. In this case one has to perform a 2D numerical integration for each value of  $k/T$  and for each value of  $m_D/T$ ; in App. A we give details on the numerical implementation. Results are shown in Fig. 3 as a solid red line. As expected, it is everywhere positive and larger than the two other curves. As the difference between this rate and the strict LO and subtraction schemes is of order  $g_3$ , it remains quantitatively distinct from these other two schemes for  $k \gtrsim T$  even at the largest temperature considered there.

We wish to emphasize again that no scheme is leading-order accurate for  $k \lesssim m_D$ , whereas for  $k \gtrsim T$  they all are, with the tuned one larger than the other two by an  $\mathcal{O}(g_3)$  amount. In the following we shall consider the spread between the rates and the ensuing axion abundances as a handle on the theory uncertainty of these leading-order calculations. We think that this uncertainty could be better quantified by a determination of the NLO  $\mathcal{O}(g_3)$  correction to the rate for  $k \gtrsim T$ , along the lines of what has been carried out in [57] for transverse momentum broadening and in [48, 65] for the photon production rate from a QCD plasma and its shear viscosity, respectively. As we briefly review in App. C, these  $\mathcal{O}(g_3)$  corrections arising from the soft  $g_3 T$  momentum scale are the root cause of the oftentimes poor convergence shown in perturbative calculations.

In light of this, we think that a conservative estimate of their possible size would in turn give a conservative handle on the effect they would have. In Eq. (A.30) we thus exploit the direct proportionality between the soft contribution to  $\Gamma(k)_{\text{KSVZ}}$  and  $\hat{q}$ , as pointed out after Eq. (2.11), to include the NLO corrections to the latter as a proxy for the size of potentially large NLO corrections to  $\Gamma(k \gtrsim T)_{\text{KSVZ}}$ . We remark that, due to this proportionality, these corrections will certainly be part of the full set of NLO corrections, whose complete determination we leave to future work. Let us furthermore note that these NLO  $\mathcal{O}(g_3)$  corrections cannot be correctly captured by the approach of [26, 36]: these corrections require proper handling of soft external states and of vertices with soft external momenta. Conversely, the vertices and propagators in their resummed, Feynman–gauge self-energy are bare and can only describe hard quasi-particles.

We conclude by noting that, once  $k \lesssim g_3^4 T$ , the quasiparticle approach implicit in Eq. (2.2) breaks down completely and one enters the so-called hydrodynamic regime. There the axion can no longer resolve particles or even HTL quasiparticles but only longer-wavelength hydrodynamical-like excitations, which are encoded in transport coefficients, i.e. the zero-frequency slope of the spectral function of the underlying conserved charges. In the case of photon production the charge would be the electromagnetic one and the transport coefficient the electrical conductivity, in the case of gravitational waves one has the energy-momentum tensor and the shear viscosity. In this case one has the topological charge and the *sphaleron*

rate, which is proportional to the thermal axion production rate at vanishing momentum [66].

Axions at such soft momenta give a very small contribution to  $\Delta N_{\text{eff}}$  — see Eqs. (4.1) and (4.3) — and once  $k \sim m_a$  they would not be dark radiation. It has however recently been proposed in [18, 19] to use non-perturbative determinations of the strong sphaleron rate up to  $k \gtrsim T$ . Let us point out that a recent parametrisation [67] of the spectral function of the topological charge finds a “transport dip” rather than a transport peak at small frequency  $\omega$ , pointing to a small contribution of the  $\omega \lesssim g_3^4 T$  region sensitive to sphaleron dynamics. It would be interesting to carry out a similar analysis for the spectral function at finite momentum, which is the relevant one for on-shell axion production.

### 3 Numerical results for the production rate

In this section we present our numerical results for the axion rate in the three schemes defined in the previous section. We refer to App. A for details on the reduction to two-dimensional numerical integrals. We use the results of [68] for the QCD running coupling, which are five-loop accurate and account for quark mass thresholds. With a renormalisation scale  $\mu = 2\pi T$  this yields  $\alpha_s(T = 300 \text{ MeV}) \approx 0.31$  and  $\alpha_s(T = 10 \text{ TeV}) \approx 0.06$ .

As per the previous section, the rate depends on  $N_f$ , the number of light quarks. To account for the effect of the electroweak phase transition giving mass to the heaviest quarks and subsequently leading to them dropping out of thermal equilibrium, we used a dynamical number of quarks flavors

$$N_f(T) = 3 + \sum_{i=c,b,t} \frac{\chi_i(T)}{\chi(m=0)}, \quad (3.1)$$

where

$$\chi_i(T) = \int \frac{d^3\mathbf{p}}{(2\pi)^3} (-2n'_F(E_i)) \quad (3.2)$$

is the susceptibility of the quark flavor  $i$  with energy  $E_i \equiv \sqrt{k^2 + m_i^2(T)}$ . There  $m_i(T)$  is the mass of quark  $i$  and  $\chi(m=0) = T^2/6$ . We use the results of [68] for the quark masses  $m_i(T)$ , which are evolved to five loops in the QCD coupling and which account for the temperature dependence of the Higgs expectation value.

In Fig. 3 we plot the rate  $\Gamma(k)$  as a function of momentum at a temperature close to the QCD transition —  $T = 300 \text{ MeV}$  — and at one above the electroweak transition,  $T = 10 \text{ TeV}$ . In the latter case the smaller coupling implies  $m_D/T \approx 1$ , indicated by the vertical line for  $k = m_D$ . For  $k > m_D$  we see that the three schemes are close, and that they respect our expectations: the strict LO and subtraction are much closer to each other than to the tuned mass scheme. Indeed, as we explained, for  $k \gtrsim T$  the strict LO and subtraction scheme differ by  $\mathcal{O}(g_3^2)$ , while the tuned mass one is  $\mathcal{O}(g_3)$  apart from them. At  $T = 300 \text{ MeV}$  the correspondingly larger coupling shows well the effect of the extrapolation to larger couplings and to  $k \lesssim m_D$ . In this case the  $k$  range giving rise to negative rates is much larger and the spread between the tuned mass and the other schemes more pronounced.

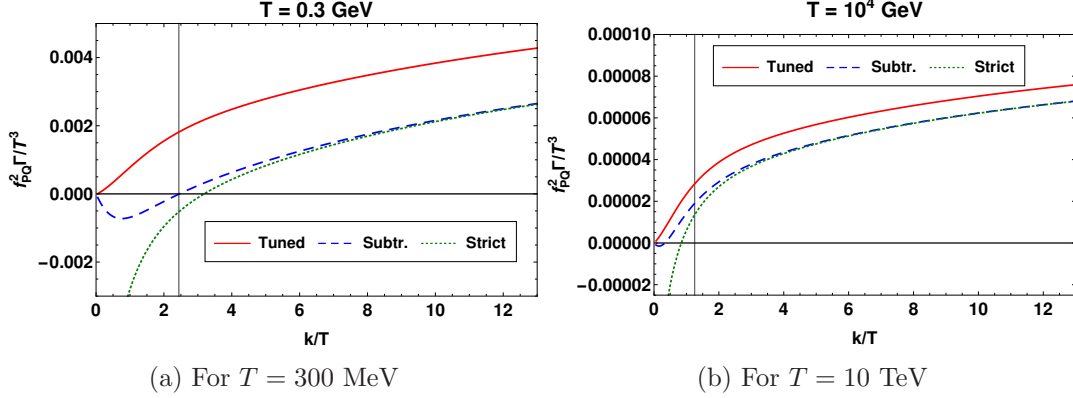


**Figure 3:** Production rate for all schemes at fixed  $T$  as a function of the axion momentum  $k$ . The strict LO (“Strict”), subtraction (“Subtr.”) and tuned mass schemes (“Tuned”) are defined in Eqs. (2.13), (2.17) and (2.18) respectively. See the main text for the choice of couplings and quark mass thresholds. The vertical line corresponds to  $k = m_D$ .

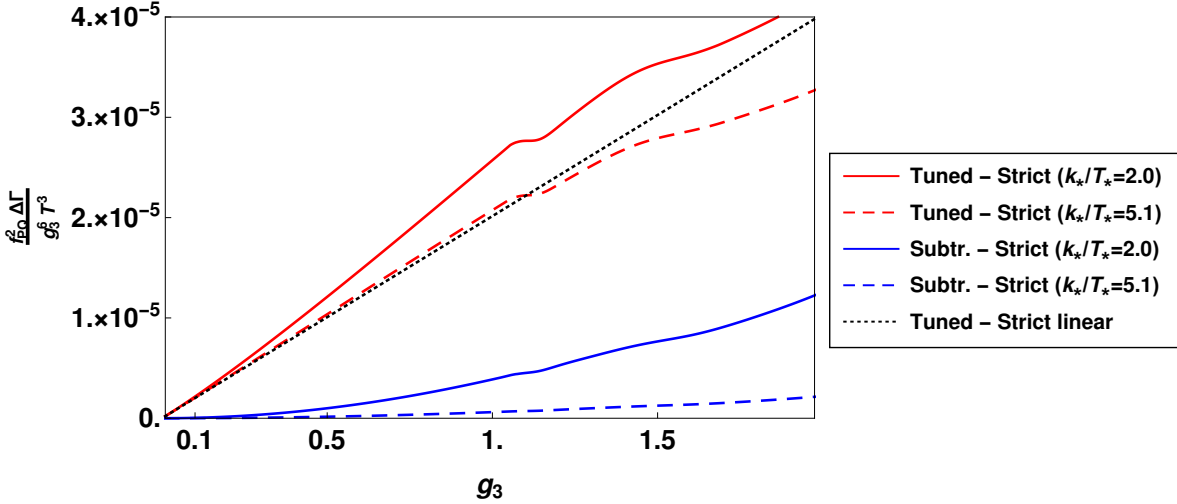


**Figure 4:** The difference between the rate in different schemes as a function of the coupling  $g_3$ . We normalise the vertical axis by the leading power of the coupling,  $g_3^6$ , and by the dimensionful factor  $T^3/f_{PQ}^2$ . We choose two momenta for which  $k \gtrsim T$ . See the main text for the definition of the “Tuned - Strict linear” curve. The step-like features stem from changes in  $N_f(T)$  through Eq. (3.1).

To further highlight the deviations between the three schemes, in Fig. 4 we plot their difference normalised by the leading power of the coupling,  $g_3^6$ , and by the dimensionful factor  $T^3/f_{PQ}^2$ . The plot then clearly shows how the tuned scheme differs from the other two by an  $\mathcal{O}(g_3)$  amount. This is made particularly evident by the “Tuned - Strict linear” curve in dotted black. It shows the leading,  $\mathcal{O}(g_3)$  contribution to the difference between the tuned

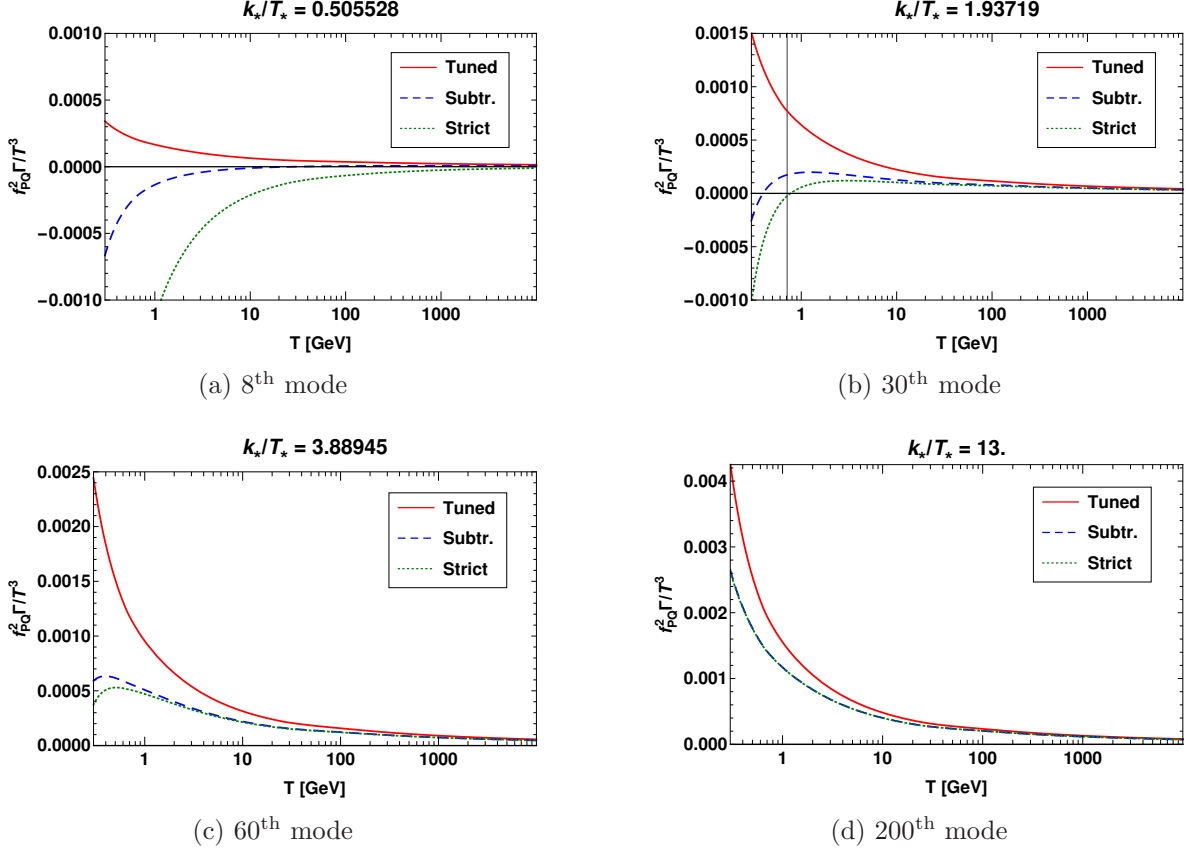


**Figure 5:** Production rate for all schemes at fixed  $k_*$  as a function of the temperature, for a few test modes. The vertical line corresponds to the temperature for which  $k(T) = m_D(T)$ . In Fig. 5a this happens for  $T > T_{\max}$ , whereas in Figs. 5c–5d this happens for  $T < T_{\min}$ .

and strict schemes. It is computed analytically in App. A, where it is given by Eq. (A.26). It is momentum-independent.

In preparation for the solution of the rate equation, Eq. (1.1), we proceed to tabulate the rates on a grid of temperature and comoving momentum. For the former we pick 300 logarithmically spaced points between  $T_{\min} = 300$  MeV and  $T_{\max} = 10$  TeV, with 200 values below the electroweak crossover  $T_{\text{EW}} = 160$  GeV and 100 values above. We define the (normalized) comoving momenta at a reference temperature  $T_* = T_{\min}$  as 200 evenly spaced points between  $k_{\min}/T_* = 0.05$  and  $k_{\max}/T_* = 13$ . For every other temperature, the momenta are blue-shifted using the relation

$$\frac{k(T)}{T} = \frac{k_*}{T_*} \left( \frac{s(T)/T^3}{s(T_*)/T_*^3} \right)^{1/3}, \quad (3.3)$$

where  $k_*$  is the value of  $k$  at  $T_*$  and  $s(T)$  is the SM entropy density, tabulated in [69] accounting for interactions and quark mass thresholds.



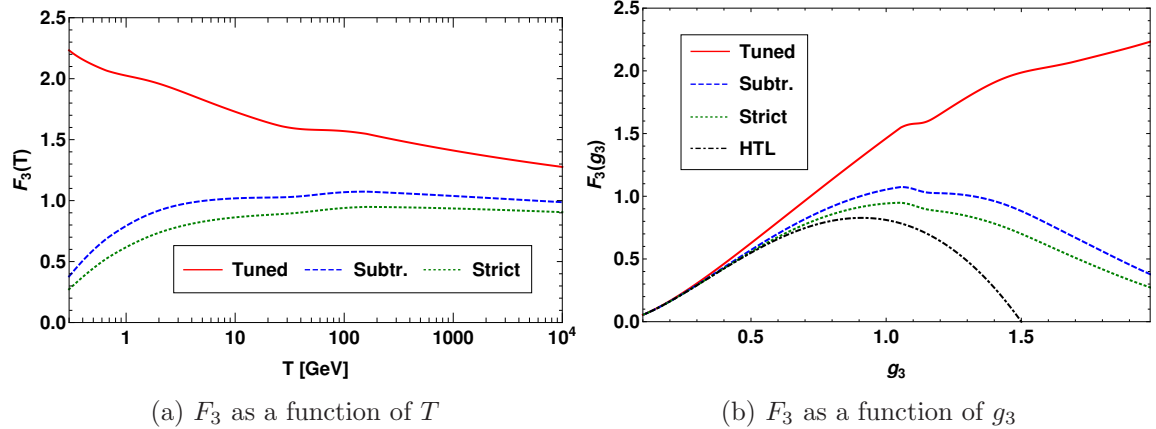


**Figure 6:** Momentum-averaged rate  $F_3$  for all three computational schemes. See the main text for the definition of  $F_3$  and for more remarks on the “HTL” curve in Figure 6b. The step-like features in the two plots stem from changes in  $N_f(T)$  through Eq. (3.1).

Numerical results obtained for the production rate, as well as for other quantities of phenomenological interest defined in Section 4, have been made available on ZENODO [70].

In Fig. 5 we now present some results for the production rate with respect to  $T$  at fixed  $k_*$ . This figure confirms the finding of Fig. 3, namely that in the region of validity of the calculations, i.e.  $k \gtrsim T$ , the strict LO and subtraction schemes agree perfectly. On the other hand, when  $k \lesssim m_D$  or, in the low  $T$ , high  $g_3$  region,  $k \sim T \sim m_D$ , both methods yield unphysical negative rates. However, it can be seen from Figures 3b and 5b for example that the region where the subtraction production rate is negative is smaller than the region where the strict LO rate is negative. The subtraction method also manages to keep the negative values at a more acceptable level, see *e.g.* Figure 3b where the negative dip around  $k = 0$  is barely visible.

Next, we compute and plot the momentum average  $\langle \Gamma \rangle$  of the rate, defined as

$$\langle \dots \rangle \equiv \frac{\int \frac{d^3\mathbf{k}}{(2\pi)^3} n_B(k) (\dots)}{\int \frac{d^3\mathbf{k}}{(2\pi)^3} n_B(k)}. \quad (3.4)$$

In the interest of comparisons with previous works, we recast it in the form of  $F_3(T)$  in [26, 28]. Adapting it to our notation, it is expressed as:<sup>7</sup>

$$F_3(T) = \frac{512\pi^5 f_{\text{PQ}}^2 \langle \Gamma \rangle}{(N_c^2 - 1) g_3^4(T) T^3}. \quad (3.5)$$

<sup>7</sup>Readers may have noticed that (3.5) is lacking the 1PI effective coefficient  $\tilde{c}_g^\Psi(T)$  present in [28]. This is because we consider the situation  $T \ll m_\Psi$ , with  $m_\Psi$  the mass of the heavy KSVZ fermion. In this regime  $\tilde{c}_g^\Psi(T) \rightarrow 1$ .

Numerical results for  $F_3$  for all considered computation schemes are plotted in Fig. 6. A comparison with the so-called “HTL” rate is also provided. This rate is defined in [26] as

$$F_3^{\text{HTL}} = g_3^2 \ln \left( \frac{1.5^2}{g_3^2} \right). \quad (3.6)$$

It corresponds to the strict LO scheme of [25] with constant  $N_f = 6$ . One important thing to note for the integral in (3.4) is that, as we shall motivate in the next Section, we exclude momentum regions giving rise to unphysical negative rates from the integration range. This is different from what is done in [25] — see also footnote 10. This is why  $F_3^{\text{HTL}}$  becomes negative for  $g_3 \gtrsim 1.5$ . Conversely, in the weak-coupling limit,  $g_3 \rightarrow 0$ , we have  $N_f(T) \rightarrow 6$  and we are also in the region of validity of the strict LO approach, so  $\langle \Gamma \rangle$  remains positive. We therefore expect our results to converge towards (3.6). As we can see on Figure 6b this is indeed what happens. One also sees clearly once more the difference between the  $\mathcal{O}(g_3^2)$  spread of the subtraction and strict LO curves and their  $\mathcal{O}(g_3)$  difference with the tuned mass one.

Moreover, we remark that the values of  $F_3$  resulting from the gauge-dependent scheme of [26] with its aforementioned pathologies are significantly larger. [26] finds  $F_3 \approx 5$  for  $g_3 \approx 1.1$ , which is 3 to 5 times larger than our results. The numerical implementation of this scheme in [28] results in  $F_3(T = 10^4 \text{ GeV}) \approx 3$  and  $F_3(T = 2 \text{ GeV}) \approx 16.5$ . Our values for the tuned mass scheme are a factor of 2 lower at  $T = 10^4 \text{ GeV}$  and a factor of 8 lower at  $T = 2 \text{ GeV}$ . As we mentioned, in App. B we argue that the gauge-dependent resummation performed in [26] introduces an unphysical, gauge-dependent sensitivity to the chromomagnetic non-perturbative scale  $g_3^2 T$  [54]. This sensitivity shows up as an extra double-pole divergence, whose numerical handling in [26, 28] is at the moment unclear. Our position is that these results are not to be trusted, as they most likely rely on some form of numerical regularisation of a genuine, non-integrable divergence.

Finally, let us give a first assessment of the possible size of NLO corrections. As we explained at the end of the previous section, in Eq. (A.30) we just add the very large  $\mathcal{O}(g_3)$  corrections to  $\hat{q}$  to the strict LO rate, to act as a proxy for the expected large NLO corrections. As that equation shows, this  $\mathcal{O}(g_3)$  contributions amounts to a positive, momentum-independent factor multiplying  $g_3^7 T^3 / f_{\text{PQ}}^2$ , which thus shift the rate upwards for all momenta. We find that for  $T = 10^4 \text{ GeV}$  the value of  $F_3$  from our NLO Ansatz is twice that from the tuned scheme. At our lowest value,  $T = 300 \text{ MeV}$ , the NLO Ansatz  $F_3$  is almost 9 times larger than its counterpart from the tuned scheme.

As expected, our Ansatz results in very large corrections, which overtake any LO-equivalent scheme even at our highest temperature, reproducing the behaviour already observed in thermal QCD calculations [57]. In the next section we will see the effect that these potential corrections would have on  $\Delta N_{\text{eff}}$ . Here we remark that it has been suggested, in the hot QCD literature, that the apparent poor convergence may arise from an overscreened LO rather than from large NLO corrections [71, 72] — see App. C for more details. Efforts are currently underway in [73, 74] to determine the soft contribution to  $\hat{q}$  — and hence to the axion rate —

non-perturbatively to all orders. These first results suggest that the non-perturbative value should be smaller than the large, perturbative NLO one. We plan to return to this issue in a future publication.

#### 4 Momentum-dependent axion freeze-out above the QCD crossover

We now turn to the evaluation of the phenomenological quantity of interest  $\Delta N_{\text{eff}}$ , which measures the impact of thermal axion production on the total energy density of the Universe. It is defined as

$$\Delta N_{\text{eff}} = \frac{8}{7} \left( \frac{11}{4} \right)^{4/3} \frac{e_a(T_{\text{CMB}})}{e_\gamma(T_{\text{CMB}})}, \quad (4.1)$$

where  $e_a$  is the axion energy density,  $e_\gamma$  is the photon energy density (from the Cosmic Microwave Background) and  $T_{\text{CMB}} \approx 0.3$  eV is the decoupling temperature of the CMB. The number and energy densities of a (massless) particle  $X$  are defined as:

$$n_X = g_X \int \frac{d^3\mathbf{k}}{(2\pi)^3} f_X(k), \quad (4.2)$$

$$e_X = g_X \int \frac{d^3\mathbf{k}}{(2\pi)^3} k f_X(k), \quad (4.3)$$

where  $f_X$  is the phase-space distribution of  $X$  and  $g_X$  its degeneracy.

The most natural way to obtain  $\Delta N_{\text{eff}}$  is to solve the momentum-dependent Boltzmann equation, Eq. (1.1), which we can rewrite as

$$\frac{df_a(k(T))}{d \ln(T_*/T)} = \frac{\Gamma(k(T))}{3H(T)c_s^2(T)} [n_{\text{B}}(k(T)) - f_a(k(T))], \quad (4.4)$$

where  $T_* = T_{\text{min}}$  is our lower temperature. We have used that  $dT = -3TH(T)c_s^2(T)dt$  and we have rewritten it in terms of comoving momenta, defined in Eq. (3.3), to remove the explicit Hubble term from Eq. (1.1).  $H(T) = \sqrt{8\pi e(T)/(3m_{\text{Pl}}^2)}$  is the Hubble rate —  $e(T)$  is the energy density and  $m_{\text{Pl}}$  the Planck mass — and  $c_s^2(T)$  is the speed of sound squared. We follow the values tabulated in [69], which account for interactions, the electroweak transition and the quark mass thresholds.<sup>8</sup>

We choose our initial temperature  $T_{\text{max}} \ll f_{\text{PQ}}$  so that the effective Lagrangian (2.1) is applicable. We also require that  $T_{\text{max}}$  is large enough that  $\Gamma/H \gg 1$  for all  $k$  there, so that axions are in thermal equilibrium. Eq. (4.4) needs then to be integrated from the initial condition  $f_a(k(T = T_{\text{max}})) = n_{\text{B}}(k(T = T_{\text{max}}))$  to  $T_{\text{min}}$ . If  $\Gamma(k)/H(T_{\text{min}}) \ll 1$  for all  $k$  there and at all later temperatures, then the axion yield  $Y_a = n_a/s$  or the comoving axion energy

---

<sup>8</sup>This only accounts for SM degrees of freedom. We thus neglect the axion's own contribution to the energy density of the universe. As we restrict ourselves to temperatures above the QCD transition, this corresponds to a percent-level uncertainty.

density<sup>9</sup>  $\tilde{e}_a = e_a/s^{4/3}$  will no longer evolve afterwards. Eq. (4.1) can then be rewritten as

$$\Delta N_{\text{eff}} = \frac{8}{7} \left( \frac{11}{4} \right)^{4/3} \frac{s^{4/3}(T_{\text{CMB}})}{s^{4/3}(T_{\text{min}})} \frac{e_a(T_{\text{min}})}{e_\gamma(T_{\text{CMB}})}. \quad (4.5)$$

We remark that the individual momentum modes are uncoupled in Eq. (4.4), which can then be solved mode by mode. We can then integrate  $f_a(k(T_{\text{min}}))$  with respect to  $k$  to obtain the energy density and thence  $\Delta N_{\text{eff}}$  from Eq. (4.5). We will comment later on the choice of  $T_{\text{min}}$  with respect to the condition  $\Gamma(k)/H(T_{\text{min}}) \ll 1$  for all  $k$ .

In what follows we will not only quantify the theoretical uncertainty from the different schemes introduced in Sec. 2, but also that arising from adopting the commonly used *momentum-averaged approximation*. It follows by assuming that, even during and after freeze out, axions are in kinetic equilibrium with a multiplicative, temperature-dependent factor. While such an approximation is well justified in the classic case of WIMP freeze out [75], where the processes responsible for chemical and kinetic equilibrium are different, it is not a priori clear if this is true in our case. Under that assumption, one sets  $f_a(k(T)) = f_a(T)n_B(k(T))$  and integrates the Boltzmann equation with respect to  $k$ . One can then directly obtain an equation for  $Y_a$

$$\frac{dY_a(T)}{d \ln(T_*/T)} = \frac{\langle \Gamma \rangle(T)}{3H(T)c_s^2(T)} [Y_{\text{eq}}(T) - Y_a(T)], \quad (4.6)$$

and for  $\tilde{e}_a$

$$\frac{d\tilde{e}_a(T)}{d \ln(T_*/T)} = \frac{\langle \Gamma k \rangle(T)n_{\text{eq}}(T)}{3H(T)c_s^2(T)e_{\text{eq}}(T)} [\tilde{e}_{\text{eq}}(T) - \tilde{e}_a(T)], \quad (4.7)$$

where  $Y_{\text{eq}}(T) = n_{\text{eq}}(T)/s(T)$  and  $\tilde{e}_{\text{eq}}(T) = e_{\text{eq}}(T)/s^{4/3}(T)$ , with  $n_{\text{eq}}(T) = \zeta(3)T^3/\pi^2$  and  $e_{\text{eq}}(T) = \pi^2T^4/30$ . The definition of the momentum average  $\langle \dots \rangle$  has been given in Eq. (3.4). The initial conditions are  $Y_a(T_{\text{max}}) = Y_{\text{eq}}(T_{\text{max}})$  for (4.6) and  $\tilde{e}_a(T_{\text{max}}) = \tilde{e}_{\text{eq}}(T_{\text{max}})$  for (4.7). When solving Eq. (4.7) one can again directly use its resulting value of  $e_a(T_{\text{min}})$  in Eq. (4.5). If, on the other hand, Eq. (4.6) is solved, as in [27, 28], one needs to introduce and determine the decoupling temperature  $T_{\text{D}}$ . It follows from the assumption that the axion undergoes a freeze-out and decouples instantaneously from the thermal bath, at  $T = T_{\text{D}}$ . Under this approximation one finds (see e.g. [28])

$$\Delta N_{\text{eff}} = \frac{4}{7} \left( \frac{11}{4} \right)^{4/3} \left( \frac{g_{*s}^{\text{SM}}(T_{\text{CMB}})}{g_{*s}^{\text{SM}}(T_{\text{D}})} \right)^{4/3}, \quad (4.8)$$

where we have used the usual parametrization  $s = 2\pi^2 g_{*s} T^3/45$  of the entropy density, with  $g_{*s}^{\text{SM}}$  the effective number of entropy degrees of freedom in the SM. We employ the results from [69]; as in footnote 8, we neglect the axion's contribution to the entropy density.

Under this assumptions  $Y_a$  stays equal to a limit value  $Y_\infty$  it had when the axion decoupled from the thermal bath, yielding

$$Y_\infty = \frac{n_a(T_{\text{D}})}{s(T_{\text{D}})} = \frac{1}{s(T_{\text{D}})} \int \frac{d^3\mathbf{k}}{(2\pi)^3} n_B(k) = \frac{\zeta(3)T_{\text{D}}^3}{\pi^2 s(T_{\text{D}})} = \frac{45\zeta(3)}{2\pi^4 g_{*s}^{\text{SM}}(T_{\text{D}})}, \quad (4.9)$$

---

<sup>9</sup>The normalization by the appropriate power of the entropy density was taken to factor out the effect of the expansion of the universe from the evolution of the values of  $n_a$  and  $e_a$ .

which can be inverted numerically. The resulting value for  $g_{*s}^{\text{SM}}(T_{\text{D}})$  can then be plugged in Eq. (4.8).

As we anticipated at the end of the previous section, we have chosen to avoid unphysical results by simply putting  $\Gamma$  to 0 whenever the computed value is negative. This applies to Equation (4.4), as well as to the computation of  $\langle\Gamma\rangle$  and  $\langle\Gamma k\rangle$  that enter Equation (4.6) and (4.7) respectively. As shown in Fig. 6b,  $\langle\Gamma\rangle$  in the strict LO scheme had been determined in [25] including the contribution of negative unphysical rates, so our treatment here is slightly different.<sup>10</sup>

We studied the dependence of  $\Delta N_{\text{eff}}$  on  $f_{\text{PQ}}$  in the range above  $f_{\text{PQ}}^{\text{min}} = 10^8$  GeV. This lower bound was chosen close to the  $f_{\text{PQ}} \gtrsim 4 \times 10^8$  GeV bound from the observation of neutrinos emitted by SN1987A, as obtained in [76]. See also [77] for a more recent and complete review of the current bounds on  $f_{\text{PQ}}$ , including the aforementioned [76]. We note that all other bounds (*e.g.* from neutron star cooling) are less constraining. Figure 7 shows the final results for  $\Delta N_{\text{eff}}$ . As one can see, for values  $f_{\text{PQ}} \gtrsim 10^9$  GeV the freeze out happens well above the electroweak phase transition, where  $\Delta N_{\text{eff}}$  becomes essentially temperature-independent in a SM bath.

We further note that it was argued recently in [20] that, in non-axionic benchmark models for dark radiation, the absolute error on  $\Delta N_{\text{eff}}$  induced by using the momentum-averaged approximation instead of the momentum-dependent method may sometimes exceed the sensitivity of future surveys, a good example of which is CMB-S4 [11–13] which expects to be able to constrain  $\Delta N_{\text{eff}} < 0.06$  at  $2\sigma$ . This is not reflected in our analysis. We find that the momentum-dependent and averaged determinations of  $e_a$  within the same scheme correspond to at most an absolute error of  $5.0 \times 10^{-4}$  for  $\Delta N_{\text{eff}}$ . On the other hand, the difference between momentum-dependent and  $Y$ -based determinations within the same scheme is at most  $1.9 \times 10^{-3}$ . These values arise from  $f_{\text{PQ}} = 10^8$  GeV. For the smallest allowed value  $f_{\text{PQ}} = 4 \times 10^8$  GeV these numbers turn into  $6.7 \times 10^{-5}$  for the absolute error between the momentum-dependent and momentum-averaged determinations, and  $1.9 \times 10^{-4}$  for the absolute error between the momentum-dependent and  $Y$ -based determinations.

Figure 7 also shows clearly that the choice of the computational scheme introduces a greater uncertainty than the error introduced by momentum averaging, as the difference between two schemes for the momentum-dependent method is at most  $2.6 \times 10^{-3}$  for  $f_{\text{PQ}} = 10^8$  GeV and  $2.8 \times 10^{-4}$  for  $f_{\text{PQ}} = 4 \times 10^8$  GeV. Fig. 8 shows instead the effect of the potentially large NLO corrections on  $\Delta N_{\text{eff}}$ . For the smallest allowed value  $f_{\text{PQ}} = 4 \times 10^8$  GeV the absolute spread between the strict LO and the NLO Ansatz is  $2.0 \times 10^{-3}$ , corresponding to a 7% effect on the former. As we push into lower, disallowed values of the axion scale, we see that the band rapidly grows to a 40% effect, to which the effect of delayed production at the QCD transition, discussed at the end of this section, would need to be added.

---

<sup>10</sup>Including the negative contribution can be justified in the context of the momentum-averaged approximation, where it could even be compared against the result obtained by excluding nonphysical rates. However, as we aim at comparing the solutions of Eq. (4.4) with its momentum-averaged approximations (4.6) and (4.7), we consistently exclude non-physical rates everywhere.

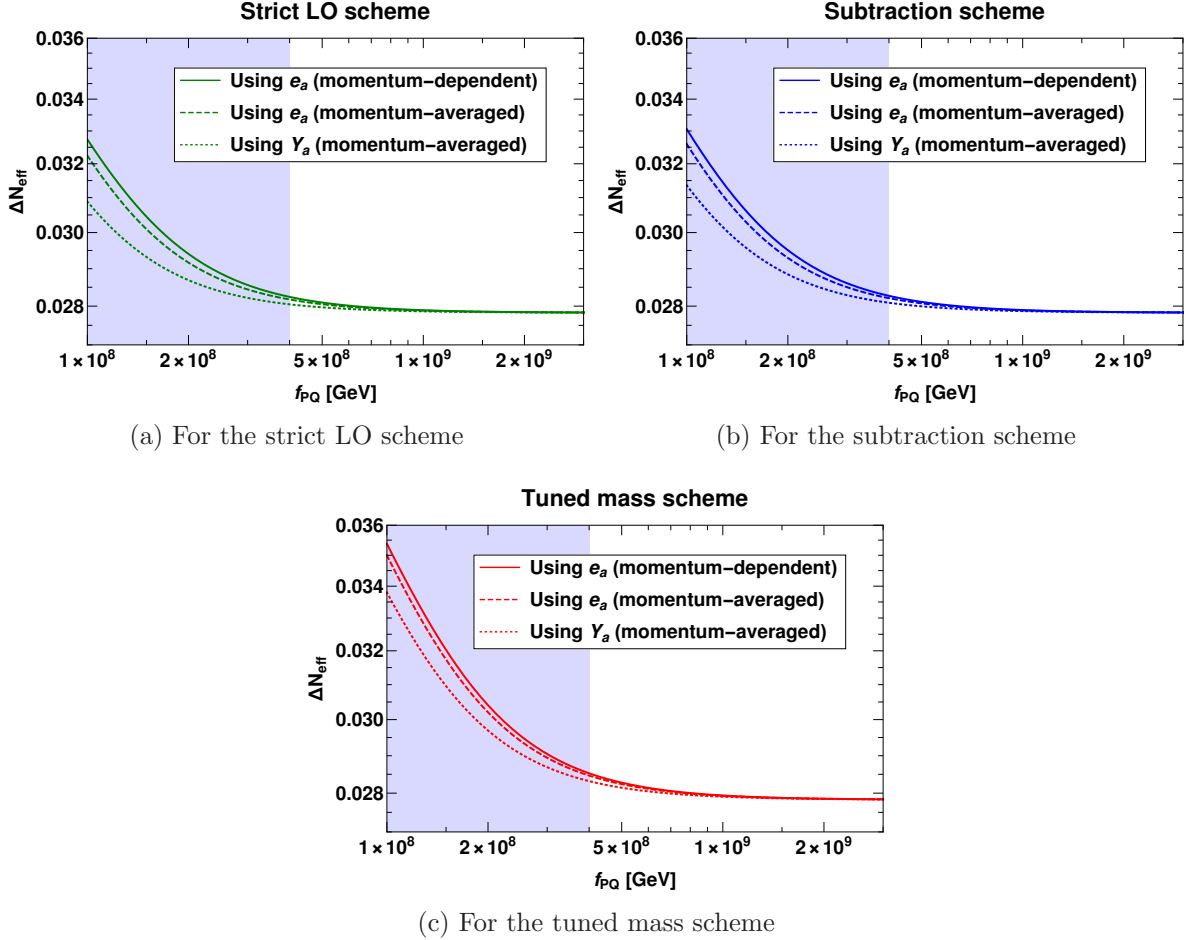


**Figure 7:** Contribution to the effective number of neutrinos as a function of  $f_{\text{PQ}}$ . Each plot uses a different scheme for the determination of the interaction rate. Within each scheme we compare the full solution of Eq. (4.4), corresponding to the “momentum-dependent” label, with results coming from the solution of the momentum-averaged approximations for  $\tilde{e}_a$ , Eq. (4.7), and for  $Y_a$ , Eq. (4.6). As explained in the main text, this last method requires the determination of  $T_{\text{D}}$  and relies on a very rapid freeze out. The shaded region corresponds to the values of  $f_{\text{PQ}}$  excluded by the astrophysical limit in [76]. Please note that the scale of the  $y$  axis is the same on all plots.

Though the choice of computational scheme induces a larger, potentially much larger uncertainty than momentum averaging, the momentum-dependent method is still better suited for precise computations as it accounts for *spectral distortions*, i.e. momentum-dependent deviations from the equilibrium Bose–Einstein distribution that follow from different momenta decoupling at different times. The momentum-averaged approximation, conversely, relies on the assumption that the axion phase space density can be written as  $f_a(k, T) = n_{\text{B}}(k) f_a(T)$  and does not account for spectral distortions.

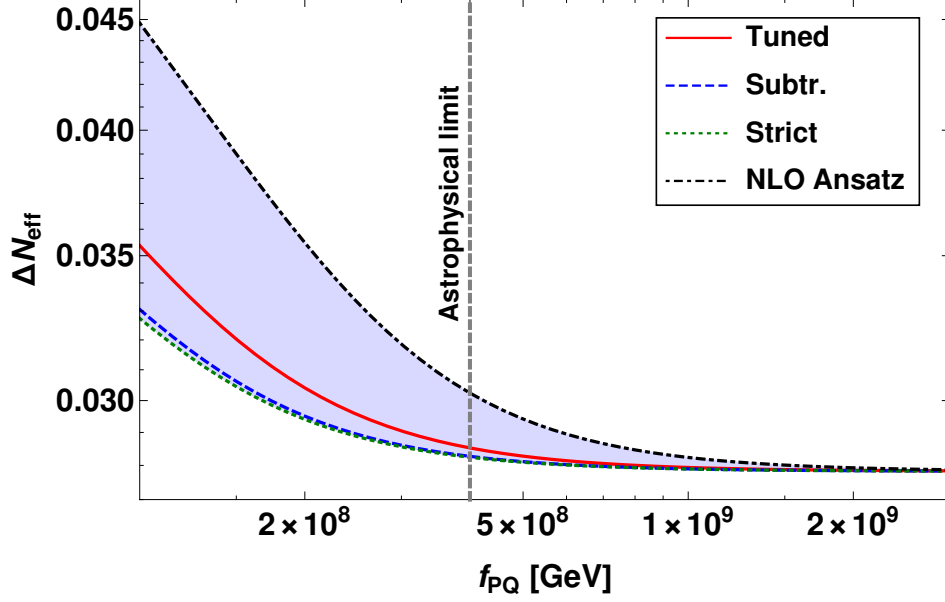
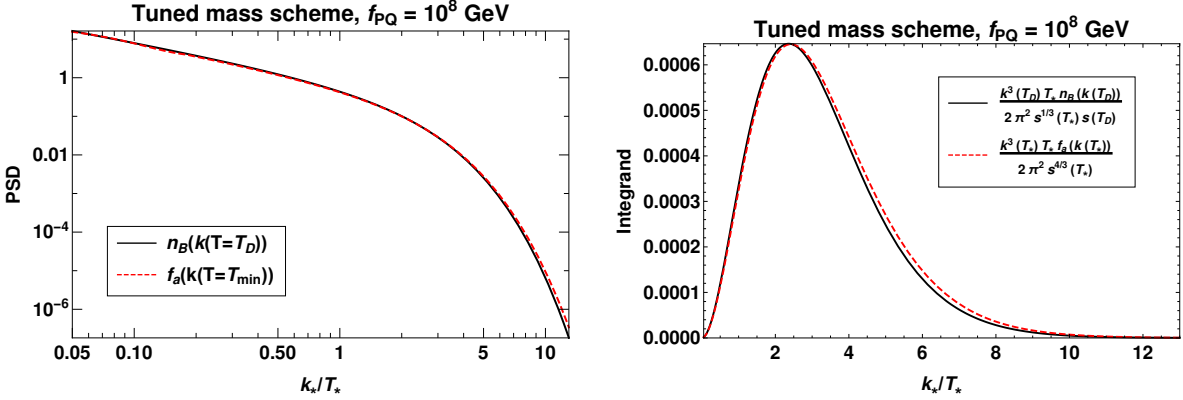


**Figure 8:** Contribution to the effective number of neutrinos as a function of  $f_{\text{PQ}}$ . All curves are obtained from the corresponding rates through the full, momentum-dependent solution of Eq. (4.4). The shaded band corresponds to a conservative estimate of the contribution of unknown, potentially large NLO corrections to  $\Gamma(k)_{\text{KSVZ}}$ , which range from the strict LO to the NLO Ansatz given in Eq. (A.30).



(a) Comparison between the axion phase space distribution at  $T = T_{\text{min}}$  and the Bose–Einstein distribution at  $T = T_{\text{D}}$ .

(b) Integrand of  $\tilde{\epsilon}_a$ , compared between  $T = T_{\text{min}}$  and  $T = T_{\text{D}}$  where in the latter case  $f_a$  has been replaced by  $n_{\text{B}}$ .

**Figure 9:** Effects of the spectral distortions on the distribution  $f_a$  and on its third moment, which is proportional to the integrand for the comoving energy density  $\tilde{\epsilon}_a$ .

In Figure 9 we quantify the impact of spectral distortions. On the left we show the axion phase space distribution  $f_a$  at  $T_{\text{min}}$  and the (equilibrium) Bose–Einstein distribution

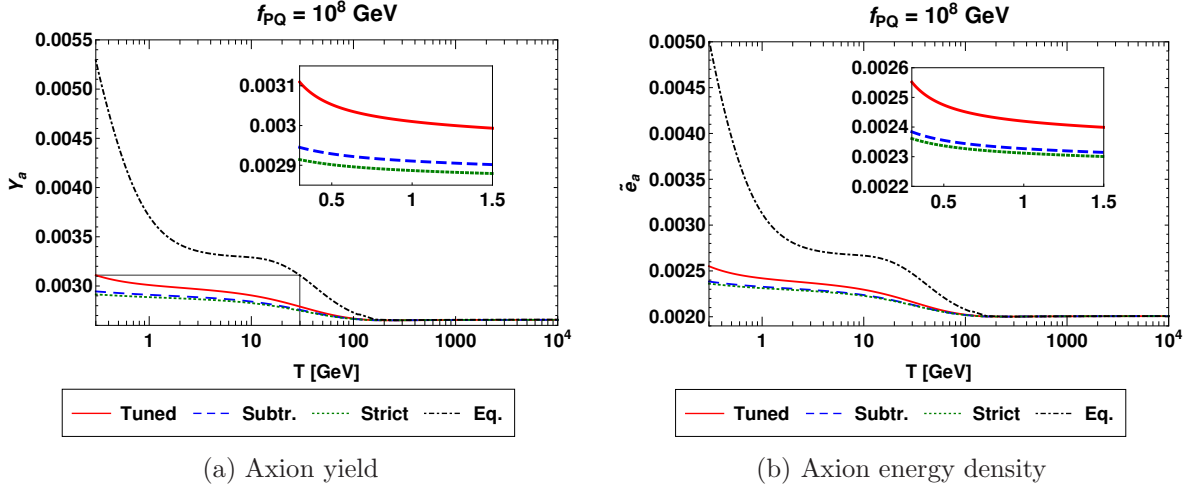


**Figure 10:** Yield and comoving energy density obtained from the momentum-dependent rates and  $f_{\text{PQ}} = 10^8$  GeV. The “equilibrium” value (“Eq.”) corresponds to  $Y_{\text{eq}}$  and  $\tilde{e}_{\text{eq}}$ . The gray lines on the axion yield figure correspond to the graphical determination of  $T_{\text{D}}$ , as defined by (4.9).

at  $T_{\text{D}}$  for  $f_{\text{PQ}} = 10^8$  GeV. As we can see the values of the two functions are very close, with the ratio  $f_a(k(T = T_{\text{min}}))/n_{\text{B}}(k(T = T_{\text{D}}))$  being at most  $\sim 1.9$ . This indicates the validity of the approximation that the axion phase space distribution gets “frozen” after decoupling as an equilibrium distribution at temperature  $T_{\text{D}}$ , which in turn justifies the definition of the decoupling temperature. The slight difference between the two curves at high  $k_*/T_*$  are representative of the spectral distortions mentioned previously. The difference between the two curves diminishes significantly as  $f_{\text{PQ}}$  increases, in fact already at  $f_{\text{PQ}} = 10^9$  GeV the two curves appear to perfectly overlap (in this case the ratio  $f_a(k(T = T_{\text{min}}))/n_{\text{B}}(k(T = T_{\text{D}}))$  is at most  $\sim 1.075$ ).

From Fig. 9b we can understand that spectral distortions are responsible from a feature clearly emerging from Fig. 7, i.e.  $\Delta N_{\text{eff}}$  values computed accounting for momentum dependence are always greater than those computed using the momentum-averaged approximation. In Fig. 9b we plot the integrand for the momentum integral in Eq. (4.3). One can then see how momentum modes at intermediate  $k_*/T_*$ , which dominate this momentum integral, stay in equilibrium a little longer, thanks to their larger rate, and thus increase the final energy density and  $\Delta N_{\text{eff}}$  contribution.

We remark that our determinations of  $\Delta N_{\text{eff}}$  require that  $\tilde{e}_a(T)$  or  $Y_a(T)$  are constant at  $T = T_{\text{min}}$  and below. However, in some cases the slope of the curve continues to increase as  $T \rightarrow T_{\text{min}}$ . Figure 10 shows  $Y_a$  and  $\tilde{e}_a$  for  $f_{\text{PQ}} = 10^8$  GeV. The inset plots show the situation described earlier, especially for the tuned method. As  $T$  approaches  $T_c \sim 155$  MeV,  $g_3$  increases very rapidly which can counteract  $\Gamma/H \sim \alpha_3^3 T m_{\text{Pl}}/f_{\text{PQ}}^2$  dropping due to the overall  $T^3$  driving the production rate. This rise in  $\Gamma/H$  signals the expected sensitivity to



non-perturbative effects around the QCD transition, which might cause extra, delayed axion production, as observed in [27, 28]. Hence, our current results should be considered as lower limits for  $\Delta N_{\text{eff}}$ : a proper treatment requires a study of axion production at and below the QCD phase transition. The methods presented in this article could be applied to this case as well, taking the Lagrangian of Chiral Perturbation Theory [78–80] as input. The obtained rate would need to be merged with that in the perturbative regime, along the lines of [27, 28]. We leave this to future work, together with the impact of the uncertainty arising from the NLO Ansatz or from a proper NLO determination at QCD-transition temperatures.

## 5 Conclusions

In this paper we have performed a careful analysis of the theory uncertainties associated with thermal production of hot axions whose interactions with the early universe plasma is dominated by their coupling to gluons. In Sec. 2.1 we reviewed how a naive approach based on the standard Boltzmann equation with bare LO matrix elements is insufficient. The well-known reason is that intermediate  $t$ - or  $u$ -channel gluons in these matrix elements can have arbitrarily soft momenta; at these large wavelengths, they no longer resolve the individual thermal particle constituents of the early-universe plasma. This is signaled by a would-be infrared divergence, that is addressed by incorporating collective plasma effects that arise at such long wavelengths.

In Sec. 2.2 we showed how this was carried out in [25] using Hard Thermal Loop resummation along the lines of [23]. This resulted in a *strict LO* rate, given in Eqs. (2.13) and (A.18). We then discuss how this rate is valid for hard axions with  $k \gtrsim T$  and how it extrapolates to non-physical negative rates for soft axions with  $k \lesssim m_{\text{D}} \sim g_3 T$ . In App. B we critically examine a more recent, gauge-dependent resummation scheme introduced in [26], showing that, taken at face value, it gives rise to a divergent result. We argue that this issue also affects calculations of gravitino [36] and axino [81] production which employ the same scheme. In Sec. 2.3 we instead introduce two novel resummation schemes inspired from right-handed neutrino and gravitational wave production on one hand and QCD thermalisation on the other. The former, called *subtraction*, is defined in Eqs. (2.17) and (A.17). The latter is termed *tuned mass* and it is given by Eqs. (2.18) and (A.20). It is constructed to be gauge-invariant and positive-definite for all axion momenta and to reduce to the strict LO rate for  $k \gtrsim T$  at small coupling. Thus, while still an extrapolation in the soft momentum range, we argue it is a better suited one and we consider it one of the main results of this paper. Given that the rate introduced in [26] is pathological, our tuned mass rate represents the most refined determination of the axion rate in the KSVZ model.

In Sec. 3 we plot our numerical results for the strict LO, subtraction and tuned mass schemes. At large temperatures and hard axion momenta they are close, with the spread between the tuned mass scheme and the other two larger than that between them. This is in agreement with our theoretical expectations and is shown by Figs. 3, 4 and 5. These figures also show the unphysical negative turn of the strict LO and, to a lesser extent, subtraction

schemes, which also causes the resulting rates for a given comoving momentum not to be a monotonic function of the temperature — see Figs. 5b and 5c. The momentum-averaged rates plotted in Fig. 6 show a similar behaviour: the tuned mass rate is monotonic, increasing for decreasing temperature, while the tuned and strict LO are not. While all rates agree for very small couplings, as shown in Fig. 6b, the spread between the more realistic tuned method and the other ones can be a factor of 5 close to the QCD transition. We further present an Ansatz for the axion rate at NLO in Eq. (A.30), built using NLO,  $\mathcal{O}(g_3)$  corrections [57] to a hot QCD quantity which shares the same operatorial form of the axion rate for soft gluon momenta. This Ansatz is built to give a conservatively large estimate of the size of NLO corrections, which are very large for this QCD quantity and related ones, as discussed in App. C. The momentum average of this NLO Ansatz rate can be a factor of 2 larger than the tuned mass one above the EW transition, growing to an almost tenfold increase in the vicinity of the QCD transition.

To investigate the consequences of the rates determined from these three schemes, in Sec. 4 we use them to solve the momentum-dependent Boltzmann equation (4.4) and its momentum-averaged approximations for the yield  $Y_a$  and comoving energy density  $e_a/s^{4/3}$  in Eqs. (4.6)-(4.7). In Fig. 7 we show our results for  $\Delta N_{\text{eff}}$  as a function of the axion scale. For values of  $f_{\text{PQ}}$  slightly smaller than astrophysically allowed ones and without considering any possible extra contribution from the QCD crossover and subsequent hadronic phase, we find that the absolute theory uncertainty from the scheme choice is of order 0.002, while that coming from the popular momentum-averaged approximation is slightly smaller if one uses the integrated Boltzmann equation (4.6) for  $Y_a$ . The error coming from the integrated Boltzmann equation (4.7) for  $e_a/s^{4/3}$  is instead a factor of five smaller, as one is directly computing the energy density  $e_a$  rather than having to infer it from the frozen-out  $Y_a$  yield through a decoupling temperature. Allowing for potentially large NLO,  $\mathcal{O}(g_3)$  corrections through our Ansatz, we find that the theory uncertainty from the scheme choice is  $2.0 \times 10^{-3}$  at the minimum allowed value  $f_{\text{PQ}} = 4 \times 10^8$  GeV, while it is only  $2.8 \times 10^{-4}$  if the NLO Ansatz is not included in the comparison. At lower, disallowed values it grows to 0.012. We thus consider  $2.0 \times 10^{-3}$  to be our most conservative estimate for the theory uncertainty to  $\Delta N_{\text{eff}}$  from astrophysically allowed KSVZ axion dynamics above the QCD crossover.

We consider this to be our other main result, which we interpret as follows. From a phenomenological point of view, the main axion dark radiation observable,  $\Delta N_{\text{eff}}$ , is not particularly sensitive to differences in the rates. The reason is that axions freeze out in the ultra-relativistic regime. There the equilibrium comoving number and energy densities depend on the temperature only through changes in the appropriate power of  $g_{*s}$  at the denominator, which never changes dramatically fast in a SM universe in the region above the QCD crossover we explored here. Hence, even rates differing by order 1 factors, as do our different schemes between the electroweak and QCD transition, can translate in the observed small differences in  $\Delta N_{\text{eff}}$ , which in relative terms are just below 10% for the smallest allowed value of  $f_{\text{PQ}}$ . We would like to remark that other approximations, such as neglecting the contribution of axions to the expansion rate — see footnote 8 — should be smaller than this uncertainty. We

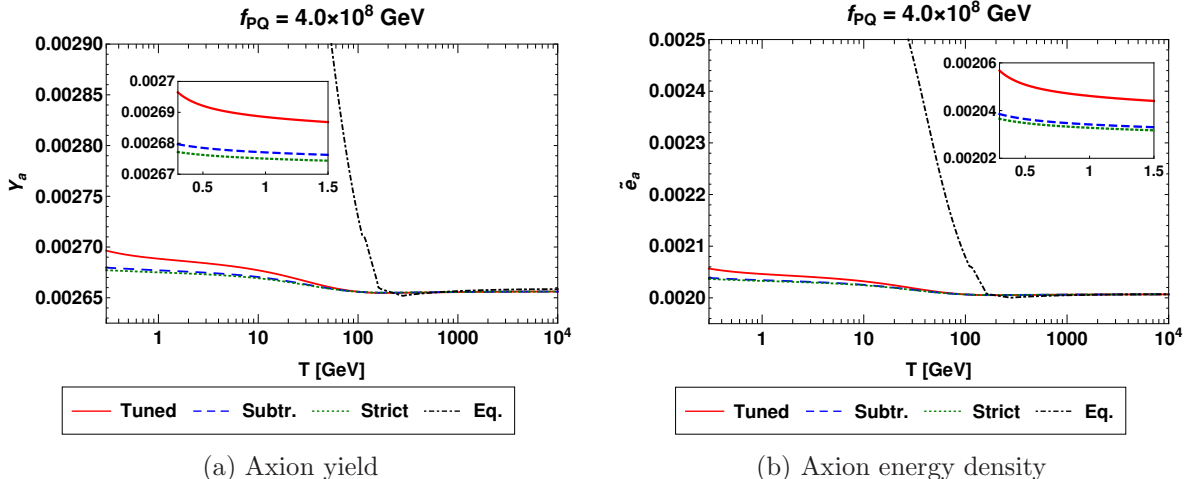


**Figure 11:** Yield and comoving energy density obtained from the momentum-dependent rates and  $f_{\text{PQ}} = 4.0 \times 10^8 \text{ GeV}$ , close to the astrophysical bound of [76]. The “equilibrium” value (“Eq.”) is defined as in 10.

would also like to point out that the impact of the different schemes would be much larger if the axions were to never reach thermal equilibrium: it would thus be interesting to perform a similar analysis for axion-like particles with a freeze-in production mechanism.

In Fig. 10 we show the temperature evolution of the yield and comoving energy density for the smallest value of  $f_{\text{PQ}}$  we considered. It shows how the resulting values, after a plateau in the 10 to 1 GeV range, start rising again when  $T$  approaches the QCD crossover. Our results for  $\Delta N_{\text{eff}}$  miss the extra axion production happening below  $T = 300 \text{ MeV}$  and are thus to be considered as lower limits. In Fig. 11 we plot the same quantities for the smallest astrophysically allowed value of  $f_{\text{PQ}}$ , showing that the emergence of the effect of the QCD transition, though less marked, is still present. We leave the interpolation of our tuned mass scheme rate with a determination in the hadronic phase and the full quantification of this delayed, off-equilibrium production to future work.

## Acknowledgements

We are indebted to Mikko Laine for sharing with us the numerical results for the running coupling and quark masses from [68]. We would also like to thank him, Francesco D’Eramo, Fazlollah Hajkarim, Seokhoon Yun, Alberto Salvio, Alessandro Strumia, Wei Xue, Guy Moore, Greg Jackson and Giulio Alvisè Dainelli for useful conversations. KB and JG acknowledge support by a PULSAR grant from the Région Pays de la Loire. JG is also funded by the Agence Nationale de la Recherche under grant ANR-22-CE31-0018 (AUTOTHERM).

## A Phase-space integrations

In this Appendix we collect useful technical details on our implementation of phase-space integrations. We remind the reader again that numerical results for the production rate, using the methods presented in this paper, are available on ZENODO [70]. Our starting point is the  $2 \leftrightarrow 2$  phase space, defined as

$$\int d\Omega_{2\leftrightarrow 2} \equiv \int \frac{d^3\mathbf{p}_1 d^3\mathbf{p}_2 d^3\mathbf{k}_1}{(2p_1)(2p_2)(2k_1)(2\pi)^9} (2\pi)^4 \delta^{(4)}(P_1 + P_2 - K_1 - K). \quad (\text{A.1})$$

In what follows we give more details on its implementation in the different schemes.

We use the parametrization of [32]. In the  $t$  channel it takes this form

$$\int d\Omega_{2\leftrightarrow 2} = \frac{1}{(4\pi)^3 k} \int_{-\infty}^k dq_0 \int_{|q_0|}^{2k-q_0} dq \int_{q_+}^{\infty} dp_1 \int_{-\pi}^{\pi} \frac{d\varphi}{2\pi}, \quad q_{\pm} \equiv \frac{q_0 \pm q}{2}, \quad (\text{A.2})$$

where  $t = q_0^2 - q^2$ ,  $K_1 = P_1 - Q$  and  $P_2 = K - Q$ . This form emerges from using the energy-conserving  $\delta$  functions to perform some angular integrations. This fixes the Mandelstam invariant  $s$  to

$$s = -\frac{t}{2q^2} \left[ (2k - q_0)(2p_1 - q_0) + q^2 - \cos(\varphi) \sqrt{(2k - q_0)^2 - q^2} \sqrt{(2p_1 - q_0)^2 - q^2} \right]. \quad (\text{A.3})$$

$u$  is easily obtained as  $u = -s - t$ .

In the  $s$  channel the form above is inconvenient, as it would put cosines of the azimuthal angle at the denominator. It is more convenient to adopt this form

$$\int d\Omega_{2\leftrightarrow 2} = \frac{1}{(4\pi)^3 k} \int_k^{\infty} dq_0 \int_{|2k-q_0|}^{q_0} dq \int_{q_-}^{q_+} dp_2 \int_{-\pi}^{\pi} \frac{d\varphi}{2\pi}, \quad (\text{A.4})$$

where  $s = q_0^2 - q^2$ ,  $P_1 = Q - P_2$  and  $K_1 = Q - K$ . The  $t$  variable becomes

$$t = \frac{s}{2q^2} \left[ (2k - q_0)(2p_2 - q_0) - q^2 + \cos(\varphi) \sqrt{q^2 - (2k - q_0)^2} \sqrt{q^2 - (2p_2 - q_0)^2} \right]. \quad (\text{A.5})$$

In the subtracted scheme we can easily take over the notation and results from [34]. Let us define

$$I_{\sigma_1\sigma_2\tau_1}^t(a_1, a_2) = \int_{q_+}^{\infty} dp_1 \int_{-\pi}^{\pi} \frac{d\varphi}{2\pi} \left[ a_1 \frac{s^2 + u^2}{t} + a_2 t \right] \frac{n_{\sigma_1}(p_1) n_{\sigma_2}(p_2) [1 + n_{\tau_1}(k_1)]}{n_{\tau_1\sigma_1\sigma_2}(p_1 + p_2 - k_1)}, \quad (\text{A.6})$$

with the expressions of  $s$ ,  $t$  and  $u$  defined in (A.3) and

$$I_{\sigma_1\sigma_2\tau_1}^s(b_1, b_2) = \int_{q_-}^{q_+} dp_2 \int_{-\pi}^{\pi} \frac{d\varphi}{2\pi} \left[ b_1 \frac{t^2}{s} + b_2 s \right] \frac{n_{\sigma_1}(p_1) n_{\sigma_2}(p_2) [1 + n_{\tau_1}(k_1)]}{n_{\tau_1\sigma_1\sigma_2}(p_1 + p_2 - k_1)}, \quad (\text{A.7})$$

with the expressions of  $s$ ,  $t$  and  $u$  defined in (A.5).  $n_{\sigma}$  is defined as

$$n_{\sigma}(k) \equiv \frac{\sigma}{e^{k/T} - \sigma}, \quad \sigma = \pm, \quad (\text{A.8})$$

such that  $n_+ = n_B$  and  $n_- = -n_F$ . The results from [34] allow us to write<sup>11</sup> for  $I^t$

$$I_{\sigma_1\sigma_2\tau_1}^t(a_1, a_2) = [1 + n_{\tau_1\sigma_1}(q_0) + n_{\sigma_2}(k - q_0)] (q^2 - q_0^2) \times \left\{ \frac{a_1[q^2 - 3(q_0 - 2k)^2][12L_3 + 6qL_2 + q^2L_1]}{6q^4} - \left(a_2 + \frac{2a_1}{3}\right)L_1 \right\}, \quad (\text{A.9})$$

where

$$L_1 \equiv T \left[ \ln(1 - \sigma_1 e^{-q_+/T}) - \ln(1 - \tau_1 e^{q_-/T}) \right], \quad (\text{A.10})$$

$$L_2 \equiv T^2 \left[ \text{Li}_2(\tau_1 e^{q_-/T}) - \text{Li}_2(\sigma_1 e^{-q_+/T}) \right], \quad (\text{A.11})$$

$$L_3 \equiv T^3 \left[ \text{Li}_3(\tau_1 e^{q_-/T}) - \text{Li}_3(\sigma_1 e^{-q_+/T}) \right]. \quad (\text{A.12})$$

For  $I^s$ , we have

$$I_{\sigma_1\sigma_2\tau_1}^s(b_1, b_2) = [n_{\tau_1}(q_0 - k) - n_{\sigma_1\sigma_2}(q_0)] (q^2 - q_0^2) \times \left\{ \frac{b_1[q^2 - 3(q_0 - 2k)^2][12(L_3^- - L_3^+) - 6q(L_2^- + L_2^+) + q^2(L_1^- - L_1^+)]}{12q^4} - \frac{b_1(q_0 - 2k)[2(L_2^- - L_2^+) - q(L_1^- + L_1^+)]}{2q^2} - \left(\frac{b_1}{3} + b_2\right)(L_1^- - L_1^+ + q) \right\}, \quad (\text{A.13})$$

where

$$L_1^\pm \equiv T \left[ \ln(1 - \sigma_1 e^{-q_\mp/T}) - \ln(1 - \sigma_2 e^{-q_\pm/T}) \right], \quad (\text{A.14})$$

$$L_2^\pm \equiv T^2 \left[ \text{Li}_2(\sigma_2 e^{-q_\pm/T}) + \text{Li}_2(\sigma_1 e^{-q_\mp/T}) \right], \quad (\text{A.15})$$

$$L_3^\pm \equiv T^3 \left[ \text{Li}_3(\sigma_2 e^{-q_\pm/T}) - \text{Li}_3(\sigma_1 e^{-q_\mp/T}) \right]. \quad (\text{A.16})$$

Going back to Eqs. (2.4) and (2.17), we get

$$\Gamma(k)_{\text{KSVZ}}^{\text{subtr}} = \frac{g_3^6(N_c^2 - 1)}{2^{13}\pi^7 f_{\text{PQ}}^2 k^2} \left\{ \int_{-\infty}^k dq_0 \int_{|q_0|}^{2k-q_0} dq \left[ N_c I_{+++}^t(-1, 0) + 2T_F N_f I_{--+}^t(1, 0) - \frac{4\pi^2 T^3 k^2 (q^2 - q_0^2)}{q^4} (N_c + T_F N_f) \right] + \int_k^\infty dq_0 \int_{|2k-q_0|}^{q_0} dq \left[ N_c I_{+++}^s(-1, 0) + T_F N_f I_{--+}^s(2, 0) \right] \right\} + \frac{g_3^4(N_c^2 - 1) T m_{\text{D}}^2}{2^{10}\pi^5 f_{\text{PQ}}^2} \ln \left( 1 + \frac{4k^2}{m_{\text{D}}^2} \right), \quad (\text{A.17})$$

---

<sup>11</sup>The decomposition used in [34] for the graviton production rate integrand, in terms of  $\frac{u^2+s^2}{t}$ ,  $t$ ,  $\frac{t^2}{s}$  and  $s$  can be applied to the axion case because the dimension of the interaction term is the same, that is dimension 5 suppressed by a mass scale. For other types of couplings a new basis would be needed.

where the sign in front of  $I_{-+-}^t$ , which is the  $q + g \rightarrow q + a$  contribution, comes from the fact that (A.6) contains  $n_-(p_1)n_+(p_2)[1 + n_-(k_1)] = -n_F(p_1)n_B(p_2)[1 - n_F(k_1)]$  which is the opposite sign compared to (2.4). We have furthermore used the identity  $\int d\Omega_{2\leftrightarrow 2}(2t+s) \dots = 0$  to simplify terms where  $\sigma_1 = \sigma_2$ .

Our implementation of the strict LO scheme, as explained in Sec. 2.3, is given by replacing  $\ln(1 + 4k^2/m_D^2)$  with  $\ln(4k^2/m_D^2)$ , i.e.

$$\Gamma(k)_{\text{KSVZ}}^{\text{strict LO}} = \Gamma(k)_{\text{KSVZ}}^{\text{subtr}} - \frac{g_3^4(N_c^2 - 1)Tm_D^2}{2^{10}\pi^5 f_{PQ}^2} \ln\left(1 + \frac{4k^2}{m_D^2}\right) + \frac{g_3^4(N_c^2 - 1)Tm_D^2}{2^{10}\pi^5 f_{PQ}^2} \ln\left(\frac{4k^2}{m_D^2}\right). \quad (\text{A.18})$$

Regarding the tuned mass scheme, it is easy to see from (2.18) that it amounts to making the following substitution in (A.17)

$$I_{\sigma_1\sigma_2\tau_1}^t(a_1, a_2) \rightarrow \frac{q^4}{(q^2 + \xi^2 m_D^2)^2} I_{\sigma_1\sigma_2\tau_1}^t(a_1, -a_1/2) + I_{\sigma_1\sigma_2\tau_1}^t(0, a_2 + a_1/2), \quad (\text{A.19})$$

and undoing the subtraction of the bare term and the addition of the HTL-resummed last line, yielding

$$\begin{aligned} \Gamma(k)_{\text{KSVZ}}^{\text{tuned}} = & \frac{g_3^6(N_c^2 - 1)}{2^{13}\pi^7 f_{PQ}^2 k^2} \left\{ \int_{-\infty}^k dq_0 \int_{|q_0|}^{2k-q_0} dq \left[ \frac{N_c q^4}{(q^2 + \xi^2 m_D^2)^2} I_{+++}^t(-1, 1/2) + N_c I_{+++}^t(0, -1/2) \right. \right. \\ & \left. \left. + 2T_F N_f \frac{q^4}{(q^2 + \xi^2 m_D^2)^2} I_{-+-}^t(1, -1/2) + 2T_F N_f I_{-+-}^t(0, 1/2) \right] \right. \\ & \left. + \int_k^\infty dq_0 \int_{|2k-q_0|}^{q_0} dq [N_c I_{+++}^s(-1, 0) + T_F N_f I_{--+}^s(2, 0)] \right\}. \quad (\text{A.20}) \end{aligned}$$

Readers familiar with [35] might wonder why we square  $q^2/(q^2 + \xi^2 m_D^2)$  in Eqs. (2.18) and (A.19)–(A.20). That is because the denominator structure of the bare diagram is a  $1/t^2$  from the gluon propagators in the amplitude and conjugate amplitude, which gets softened to a  $1/t$  by the derivatives in the axion-gluon coupling. As it is only the denominator that gets HTL-resummed, we feel that our implementation is closer to that of [59, 60], even though a non-squared factor of  $q^2/(q^2 + \xi^2 m_D^2)$  would also work, albeit with a different value of  $\xi$ . Attentive readers might have also noticed that our choice causes the  $N_c$ -proportional part to become negative for  $m_D/T \gg 1$ , where  $q^4/(q^2 + \xi^2 m_D^2)^2 \rightarrow 0$ . A straightforward modification would be to replace

$$\frac{N_c q^4 I_{+++}^t(-1, 1/2)}{(q^2 + \xi^2 m_D^2)^2} + N_c I_{+++}^t(0, -1/2) \rightarrow \frac{N_c q^4 I_{+++}^t(-1, 1)}{(q^2 + \xi^2 m_D^2)^2} + N_c I_{+++}^t(0, -1), \quad (\text{A.21})$$

in Eq. (A.20). We have checked that this results in a value of  $F_3(T_{\min})$  that is 5% larger than what we obtain from Eq. (A.20). We employ the latter in our numerics to obtain a marginally more conservative estimate of  $\Delta N_{\text{eff}}$ .

The last remaining hurdle is to find the tuning coefficient  $\xi$ . Let us now derive its numerical value. The infrared-sensitive part of the  $t$  channel integrand of  $\Gamma(k)_{\text{KSVZ}}^{\text{tuned}}$  is obtained by removing the parts that are proportional to  $t$  only (because they vanish as  $t \rightarrow 0$ ) and by expanding for  $q_0, q \sim m_{\text{D}} \ll T$ . It reads

$$\Gamma(k)_{\text{KSVZ}}^{\text{tuned}} \Big|_{\text{soft}} = \frac{g_3^6 (N_c^2 - 1) (N_c + T_F N_f) T^3}{2^{11} \pi^5 f_{\text{PQ}}^2} \int_{-\infty}^k dq_0 \int_{|q_0|}^{2k-q_0} dq \frac{q^2 - q_0^2}{(q^2 + \xi^2 m_{\text{D}}^2)^2} + \dots, \quad (\text{A.22})$$

where the dots stand for higher-order terms in the soft- $Q$  expansion. Performing the integrals and expanding the obtained result for  $k \gtrsim T$ , we obtain

$$\Gamma(k)_{\text{KSVZ}}^{\text{tuned}} \Big|_{\text{soft}} \approx \frac{g_3^4 (N_c^2 - 1) T m_{\text{D}}^2}{2^{10} \pi^5 f_{\text{PQ}}^2} \left[ \ln \left( \frac{k^2 e^{2/3}}{m_{\text{D}}^2 \xi^2} \right) + \mathcal{O} \left( \frac{m_{\text{D}}^2}{k^2} \right) \right], \quad (\text{A.23})$$

which we want to compare to the HTL contribution (2.16) in the same limit, that is

$$\Gamma(k \gtrsim T)_{\text{KSVZ}}^{\text{HTL}} \text{ [33, 34]} = \frac{g_3^4 (N_c^2 - 1) T m_{\text{D}}^2}{2^{10} \pi^5 f_{\text{PQ}}^2} \left[ \ln \left( \frac{4k^2}{m_{\text{D}}^2} \right) + \mathcal{O} \left( \frac{m_{\text{D}}^2}{k^2} \right) \right]. \quad (\text{A.24})$$

This gives  $\xi^2 = e^{2/3}/4$  or  $\xi = e^{1/3}/2$  given that we chose  $\xi$  to be positive.

As we mentioned in Sec. 2.3 and 3, the tuned scheme differs from the strict LO and subtracted ones at relative order  $g_3$ . With the detailed results of this section we can determine this  $\mathcal{O}(g_3)$  difference analytically. Let us then inspect Eqs. (A.18) and (A.20). In particular, we need to concentrate on the region of the latter equation where  $|q_0| \sim q \sim m_{\text{D}}$ : as soon as these variables become larger than  $m_{\text{D}}$ , the mass-dependent denominators in Eq. (A.20) can be expanded for  $m_{\text{D}}/T \ll 1$ , yielding deviations from the strict LO scheme that start at  $\mathcal{O}(g_3^2)$ . In the soft  $|q_0| \sim q$  regime we can then expand Eq. (A.20) for  $|q_0| \sim q \sim m_{\text{D}} \ll T$  and consider the next order after Eq. (A.22).

This next term can only come from scattering processes off gluons, as it requires a Bose–Einstein enhancement from  $n_{\text{B}}(p_1 \sim gT) \approx T/p_1 \sim 1/g$  to yield an order- $g_3$  term — see [62–64] for similar calculations. We then find

$$\begin{aligned} \Gamma(k)_{\text{KSVZ}}^{\text{tuned}} - \Gamma(k)_{\text{KSVZ}}^{\text{strict LO}} &= - \frac{g_3^6 (N_c^2 - 1) N_c T^2}{2^{12} \pi^7 f_{\text{PQ}}^2} \left\{ \int_{-\infty}^k dq_0 \int_{|q_0|}^{2k-q_0} dq \left[ \frac{1}{(q^2 + \xi^2 m_{\text{D}}^2)^2} - \frac{1}{q^4} \right] \right. \\ &\quad \times \left. \frac{(q^2 - q_0^2)(3q q_0 + (q^2 - 3q_0^2) \text{arctanh}(q_0/q))}{q_0} + \mathcal{O}(g_3^2) \right\}, \quad (\text{A.25}) \end{aligned}$$

where the massless  $q^4$  denominator on the first line comes from the strict LO scheme. The integration range can be split in the two domains  $-q < q_0 < q \wedge 0 < q < k$  and  $-q < q_0 < 2k - q \wedge q > k$ . The latter range is negligible for  $k \gtrsim T$ , as the two denominators on the first line differ by  $\mathcal{O}(g_3^2)$ . We can then concentrate on the first range; we have exploited its symmetries to drop odd terms in  $q_0$ . Furthermore, at order  $g_3$  we can extend the integration range to  $-q < q_0 < q \wedge 0 < q$ , finding that, for  $k \gtrsim T$

$$\Gamma(k)_{\text{KSVZ}}^{\text{tuned}} - \Gamma(k)_{\text{KSVZ}}^{\text{strict LO}} = 3(8 + \pi^2) \frac{g_3^6 (N_c^2 - 1) T^3}{2^{16} \pi^6 f_{\text{PQ}}^2} \left[ \frac{N_c \xi m_{\text{D}}}{T} + \mathcal{O}(g_3^2) \right]. \quad (\text{A.26})$$

Let us now introduce our Ansatz for the NLO rate with the large  $\mathcal{O}(g_3)$  corrections to the transverse momentum broadening coefficient  $\hat{q}$  determined in [57]. This reference gives the soft contribution to  $\hat{q}$  as

$$\frac{\hat{q}}{g_3^4 C_R T^3} = \frac{N_c + T_F N_f}{6\pi} \ln \frac{q^*}{m_D} + \frac{N_c}{6\pi} \frac{m_D}{T} \left[ -\frac{3q^*}{16m_D} + 3\frac{3\pi^2 + 10 - 4\ln 2}{16\pi} \right], \quad (\text{A.27})$$

where  $C_R = C_F$  for hard quark undergoing broadening and  $C_R = C_A = N_c$  for a hard gluon and  $g_3 T \ll q^*$  is the UV regulator on  $q_\perp$  to isolate the soft contribution. The linear term in  $q^*$  can be shown to cancel from an opposite contribution coming from the  $q_\perp > q^*$  range.

We now assume that the  $\mathcal{O}(g_3)$  correction to the axion rate is given by this  $\mathcal{O}(g_3)$  correction to  $\hat{q}$ . As we shall explain in App. C, it can be considered a sound estimate for the “maximal” size of NLO corrections, given that  $\hat{q}$  is the QCD observable featuring one of the largest known NLO corrections. Upon rewriting Eq. (A.24) as

$$\Gamma(k)_{\text{KSVZ}}^{\text{LL}} = \frac{g_3^6 (N_c^2 - 1) T^3}{2^8 \pi^4 f_{\text{PQ}}^2} \frac{N_c + T_F N_f}{6\pi} \ln \frac{2k}{m_D}, \quad (\text{A.28})$$

where LL stands for leading logarithm, and comparing it with Eq. (A.27) we can find the overall normalisation of  $\hat{q}$  with respect to the axion rate. We can then construct this Ansatz for the axion rate under the hypothesis of  $\hat{q}$ -like large  $\mathcal{O}(g_3)$  corrections<sup>12</sup>

$$\Gamma(k)_{\text{KSVZ}}^{\text{NLO ansatz}} \equiv \Gamma(k)_{\text{KSVZ}}^{\text{strict LO}} + \frac{g_3^6 (N_c^2 - 1) T^3}{2^8 \pi^4 f_{\text{PQ}}^2} \frac{N_c}{2\pi} \frac{m_D}{T} \frac{3\pi^2 + 10 - 4\ln 2}{16\pi}. \quad (\text{A.30})$$

We could very well have used the tuned, rather than the strict, rate, as our starting point. In that case we would have needed in principle to subtract its  $\mathcal{O}(g_3)$  contribution, as given by Eq. (A.26). In practice this is irrelevant for  $k \gtrsim T$ , given that the latter is approximately 220 times smaller than the second term on the r.h.s. of Eq. (A.30).

Finally, we remark that the  $q, q_0$  integrals can be performed numerically for all schemes to obtain the value of  $\Gamma$  for a given  $k, T$ . Note that for the subtracted and strict LO schemes the temperature dependence can be factored out of the integrals and it is therefore enough to construct an interpolator of the integral for the relevant values of  $k/T$ . The only non-multiplicative dependence on the temperature enters through the logarithmic dependence on

<sup>12</sup> For what concerns the linear term in  $q^*$ , the analysis we have carried out to obtain Eq. (A.26) can be used to show that it cancels against an opposite term hidden in the soft limit of the strict rate, i.e.

$$\begin{aligned} \Gamma(k)_{\text{KSVZ}}^{\text{strict LO } q^*} &= \frac{g_3^6 (N_c^2 - 1) T^3}{2^{11} \pi^5 f_{\text{PQ}}^2} \left\{ \int_{q^*}^{2k} dq_\perp \int_{-\infty}^{\infty} dq_0 \frac{q_\perp}{q} \frac{q_\perp^2}{q^4} \right. \\ &\quad \times \left[ N_c + T_F N_f - N_c \frac{(3qq_0 + (q^2 - 3q_0^2) \text{arctanh}(q_0/q))}{2\pi^2 q_0 T} + \mathcal{O}(g_3^2) \right] \Big\}, \\ &= \frac{g_3^6 (N_c^2 - 1) T^3}{2^8 \pi^4 f_{\text{PQ}}^2} \left[ \frac{N_c + T_F N_f}{6\pi} \ln \frac{2k}{q^*} + \frac{N_c}{6\pi} \frac{3}{16T} (q^* - 2k) \right]. \end{aligned} \quad (\text{A.29})$$

This indeed removes the linear dependence on the regulator, as expected. We have also left for illustration the logarithmic one from the LO contribution.



the coupling in the analytical term in Eqs. (2.16) and (A.17) and its strict LO limit (A.18) and is thus easily evaluated. The same is not true for the tuned mass scheme where the integration must be done for all points of the grid (see Section 3). As the operation of computing the production rate over all 60000 points of the grid can be very time-consuming, this task was performed in C using the GNU Scientific Library [82]. The C implementation of the polylogarithm functions was taken from [83].

We conclude by listing here the expressions for the Coulomb-gauge HTL-resummed gluon propagators, which have been employed in Eqs. (2.11) and Eq. (2.15). They read

$$G_R^{00}(Q) \equiv G_R^L(Q) = \frac{i}{q^2 + m_D^2 \left( 1 - \frac{q^0}{2q} \ln \frac{q^0 + q + i\epsilon}{q^0 - q + i\epsilon} \right)}, \quad (\text{A.31})$$

$$G_R^{ij}(Q) \equiv (\delta^{ij} - \hat{q}^i \hat{q}^j) G_R^T(Q) = \frac{i(\delta^{ij} - \hat{q}^i \hat{q}^j)}{q_0^2 - q^2 - m_\infty^2 \left( \frac{q_0^2}{q^2} - \left( \frac{q_0^2}{q^2} - 1 \right) \frac{q^0}{2q} \ln \frac{q^0 + q}{q^0 - q} \right)} \Bigg|_{q^0 = q^0 + i\epsilon}. \quad (\text{A.32})$$

Here  $m_\infty^2 = m_D^2/2$  is the LO gluon asymptotic mass.

## B Gauge-dependent resummations in the literature

Another purportedly positive-definite scheme was introduced in [26], extending to the axion case the work of [36] for gravitinos and of [81] for axinos. It has been used in the analysis of [27, 28]. In a nutshell, the authors compute an analogue of Fig. 2 where both propagators are resummed. Adapting their Eqs. (2.6) and (4.6) to our notation and to the labeling of Fig. 2 we find

$$\Gamma(k)^{[26]} = \frac{(N_c^2 - 1)g_3^4}{2^8 \pi^4 k f_{\text{PQ}}^2} \int \frac{d^4 Q}{(2\pi)^4} \epsilon^{\mu\nu\alpha\beta} \epsilon^{\mu'\nu'\alpha'\beta'} Q_\alpha Q_{\alpha'} (K-Q)_\beta (K-Q)_{\beta'} \frac{{}^*G_{\mu\mu'}^<(Q) {}^*G_{\nu\nu'}^<(K-Q)}{n_B(k)}, \quad (\text{B.1})$$

where  ${}^*G^<$  denotes the backward Wightman propagator, given by  ${}^*G^<(Q) = n_B(q^0) ({}^*G_R(Q) - {}^*G_A(Q))$ .  ${}^*G_R(Q)$  is the resummed retarded propagator. When the momenta  $Q$  or  $K-Q$  are space-like, the full one-loop Feynman-gauge retarded self-energy is resummed. Conversely time- and light-like momenta resum the self-energy in the HTL approximation, thus giving rise to zero-width plasmons with momentum-dependent thermal masses. This procedure is claimed to reduce to the strict LO at small  $g_3$ . It is further claimed that the gauge dependence arising from using the Feynman-gauge self-energy only enters at relative order  $g_3^2$ .

We do not agree with these claims and we now carefully scrutinize them. Let us start by

following [26] to turn Eq. (B.1) into

$$\Gamma(k)^{[26]} = \frac{(N_c^2 - 1)g_3^4}{2^{13}\pi^7 k^2 f_{\text{PQ}}^2} \int_{-\infty}^{\infty} dq^0 \int_0^{\infty} dq \int_{|q-k|}^{q+k} dp pq \frac{n_{\text{B}}(q^0)n_{\text{B}}(k-q^0)}{n_{\text{B}}(k)} \\ \left\{ (\rho_L^{FG}(Q)\rho_T^{FG}(P) + \rho_T^{FG}(Q)\rho_L^{FG}(P))[(q+p)^2 - k^2][k^2 - (q-p)^2] \right. \\ \left. + \rho_T^{FG}(Q)\rho_T^{FG}(P) \left[ \left( \frac{q_0^2}{q^2} + \frac{p_0^2}{p^2} \right) ((q^2 + p^2 - k^2)^2 + 4q^2 p^2) + 8q^0 p^0 (q^2 + p^2 - k^2) \right] \right\}, \quad (\text{B.2})$$

where  $p^0 = k - q^0$  and  $\rho^{FG}(Q) \equiv {}^*G_R(Q) - {}^*G_A(Q)$  is the Feynman-gauge spectral density. In [26] these Feynman-gauge structures take this specific form

$${}^*G_R^T(Q) = \frac{i}{Q^2 - \theta(-Q^2)\Pi_R^{\text{vac}}(Q) - \Pi_R^T(Q)}, \quad \text{with} \quad \Pi_R^T(Q) = 1/2(\delta^{ij} - \hat{q}^i \hat{q}^j)\Pi_R^{ij}(Q), \quad (\text{B.3})$$

$${}^*G_R^L(Q) = \frac{iQ^2}{q^2(Q^2 - \theta(-Q^2)\Pi_R^{\text{vac}}(Q) - \Pi_R^L(Q))}, \quad \text{with} \quad \Pi_R^L(Q) = -\frac{Q^2}{q^2}\Pi_R^{00}. \quad (\text{B.4})$$

Here

$$\Pi_R^{\text{vac}}(Q) = -\left( \frac{5}{3}C_A - \frac{4}{3}T_F N_f \right) \frac{g^2 Q^2}{(4\pi)^2} \ln \frac{q^2 - (q^0 + i\epsilon)^2}{\bar{\mu}^2}, \quad (\text{B.5})$$

is the vacuum component of the Feynman-gauge retarded self-energy. As per the prescription of [26], it is only used in the space-like regime, together with the full Feynman-gauge thermal self-energies  $\Pi_R^{L,T}(Q)$ . Above the light cone the HTL self-energies are used instead. In this appendix we will assume that any  $\Pi$  self-energy is to be understood in Feynman gauge unless otherwise specified.

Eq. (B.2) is then naturally divided into four components, which we name pole-pole, cut-cut, pole-cut and cut-pole. Pole-pole is the contribution arising from  $Q^2 > 0$  and  $P^2 = (K - Q)^2 > 0$ , when both gluons are described by their *plasmon poles* encoded in the HTL spectral functions. Conversely, the cut-cut emerges when  $Q^2 < 0$  and  $P^2 = (K - Q)^2 < 0$ , when both gluons are in the *Landau cut*, i.e. the space-like branch cut of the thermal self-energies. Finally, the pole-cut and cut-pole are the two mixed contributions.

We now consider the region where  $k \gtrsim T$  at small  $g_3$  and prove that Eq. (B.2) *does not* reduce to the strict LO result. In this region the pole-pole and cut-cut contributions are subleading. The former case is depicted in Fig. 12. There the integral in Eq. (B.2) is dominated by the region where  $q \sim p \sim T$ . Thus the longitudinal pole contribution vanishes — there are no hard longitudinal plasmons — and the transverse one approaches a constant asymptotic mass  $m_{\text{D}}^2/2 \sim g_3^2 T^2$  [44]. If the masses are exactly equal for the  $Q$  and  $K - Q$  zero-width transverse plasmons, no axion emission can happen for energy-momentum conservation. Allowing for a small, momentum-dependent deviation between the two plasmon masses gives rise to a suppressed contribution: the factor multiplying  $\rho_T^{FG}(Q)\rho_T^{FG}(P)$  is of order  $g_3^4$  or smaller. Combining this with the multiplicative  $g_3^4$  in the prefactor of Eq. (B.2) we then have that the pole-pole contribution is suppressed by at least a factor of  $g_3^2$  with respect to the strict leading order, which is  $\sim g_3^6$ .

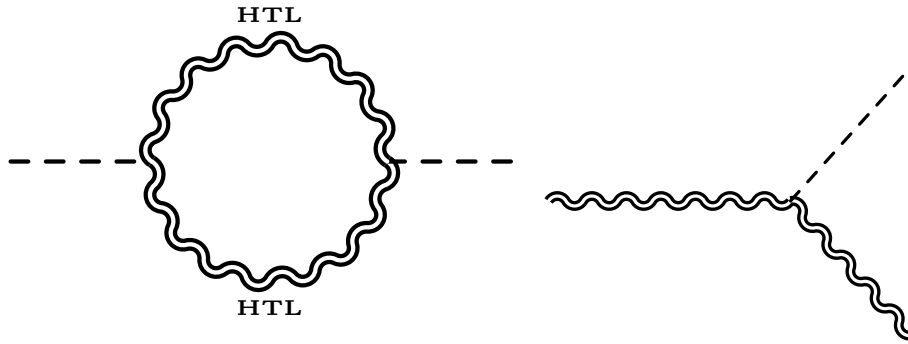


**Figure 12:** Left: the axion self-energy diagram corresponding to the pole-pole contribution. Its one cut corresponds to the square of the process shown on the right. See Sec. 2.2 for the relation between the retarded axion self-energy and the production rate.

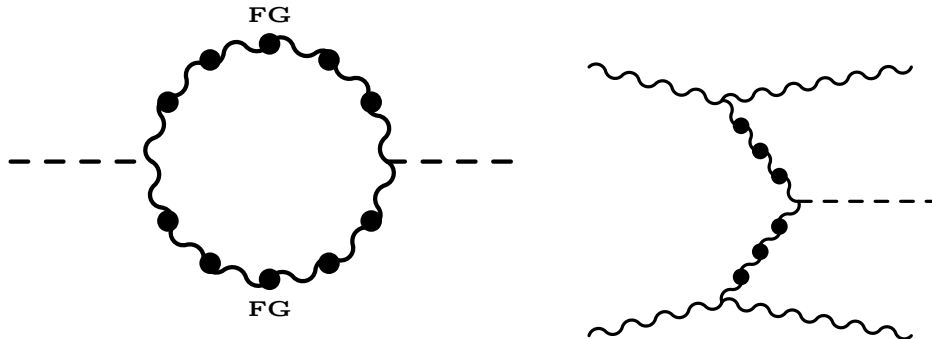


**Figure 13:** Left: the axion self-energy diagram corresponding to the cut-cut contribution. The black blobs denote the resummed self-energies in Feynman Gauge (FG). Its cut corresponds to the square of processes such as the one shown on the right. Cuts corresponding to diagrams with external quarks are not shown.

Similarly, the cut-cut contribution is also subleading, as it corresponds to higher-order  $2 \leftrightarrow 3$  processes, as shown in Fig. 13. If both  $P \sim T$  and  $Q \sim T$ , these processes are suppressed by a factor of  $g_3^2$  compared to leading order, since  $\rho(Q \sim T) \sim g^2/T^2$  in the space-like regime. For these processes to be enhanced to leading order we then need to look for regions where either  $Q$  or  $P$  are soft. Let us look at the former case for illustration: there one has  $\rho(Q) \sim 1/(g^2T^2)$  and  $\rho^T(P) \sim g/T^2$ . This latter scaling can be understood as originating from  $P = K + \mathcal{O}(gT)$ ,  $P^2 \sim gT^2$ , coupled with  $\text{Im}\Pi^T(P) \sim g^3T^2$  in this regime, as follows from Eq. (B.10). Plugging these results into Eq. (B.2) then yields that this soft-gluon contribution is also suppressed by a factor of  $g_3^2$ . Our numerical evaluation confirms this.<sup>13</sup>

<sup>13</sup>A more careful power-counting analysis shows that the cut-cut contribution should scale like  $g_3^8 \ln^2(1/g_3)$  in this non-abelian case and like  $g_3^8 \ln(1/g_3)$  in the abelian one, with the different power of the logarithm originating from the extra logarithmic sensitivity to a collinear  $P$  in the gluonic part of Eq. (B.10) compared

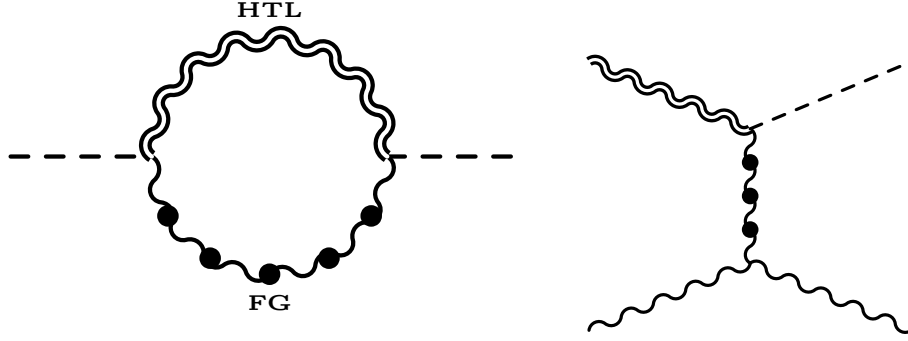


**Figure 14:** Left: the axion self-energy diagram corresponding to the pole-cut contribution. Its cut corresponds to the square of processes such as the one shown on the right. Cuts corresponding to external quarks are again not shown.

So we are then left with the pole-cut and cut-pole contributions, as shown in Fig. 14. These correspond to the  $2 \leftrightarrow 2$  processes we have treated in Sec. 2, with two notable differences. First, the intermediate gluon resums a gauge-dependent self-energy, while one of the external gluons features the HTL, rather than bare, dispersion relation. Secondly, the crossing of the diagram shown on the right in Fig. 14 into its  $s$ -channel counterpart is not possible, as it would require a time-like  $Q^2$ . These two differences are the basis of our claim that this gauge-dependent resummation does not reproduce the strict LO result for  $g_3 \ll 1$ .

To see this in detail, let us consider the sum of the pole-cut and cut-pole contributions, which is given by twice of either of the two. At small  $g_3$  and for  $k \gtrsim T$  we can again neglect the longitudinal plasmon. Hence

$$\begin{aligned} \Gamma(k)_{\text{pc+cp}}^{[26]} &= \frac{(N_c^2 - 1)g_3^4}{2^{12}\pi^7 k^2 f_{\text{PQ}}^2} \int_{-\infty}^{\infty} dq^0 \int_{|q^0|}^{\infty} dq \int_{|q-k|}^{q+k} dp pq [1 + n_{\text{B}}(q^0) + n_{\text{B}}(k - q^0)] \rho_T^{FG \text{ pole}}(P) \\ &\quad \times \left\{ \rho_L^{FG}(Q)[(q+p)^2 - k^2][k^2 - (q-p)^2] \right. \\ &\quad \left. + \rho_T^{FG}(Q) \left[ \left( \frac{q_0^2}{q^2} + \frac{p_0^2}{p^2} \right) ((q^2 + p^2 - k^2)^2 + 4q^2 p^2) + 8q^0 p^0 (q^2 + p^2 - k^2) \right] \right\}, \end{aligned} \quad (\text{B.6})$$

where we have taken  $Q$  to be the cut momentum and  $P$  the pole one.  $\rho_T^{FG \text{ pole}}$  is the pole part of the transverse spectral function. It can again be approximated by its bare one, i.e.

$$\rho_T^{FG \text{ pole}}(P \gg g_3 T) \approx 2\pi\epsilon(k - q^0)\delta((k - q^0)^2 - p^2) = \frac{\pi}{p}\epsilon(k - q^0)[\delta(p - |k - q^0|) + \delta(p + |k - q^0|)]. \quad (\text{B.7})$$

Exploiting the fact that  $Q^2 < 0$ , we find that only the  $k - q^0 > 0$  region can contribute,

---

with its quark counterpart. Our numerical evaluation confirms this scaling.

yielding

$$\Gamma(k)_{\text{pc+cp}}^{[26]} = \frac{(N_c^2 - 1)g_3^4}{2^{12}\pi^6 k^2 f_{\text{PQ}}^2} \int_{-\infty}^k dq^0 \int_{|q_0|}^{2k-q^0} dq q [1 + n_{\text{B}}(q^0) + n_{\text{B}}(k - q^0)] (q^2 - q_0^2) \times \left\{ \rho_L^{FG}(Q) [(2k - q_0)^2 - q^2] + \rho_T^{FG}(Q) \left(1 - \frac{q_0^2}{q^2}\right) [(2k - q_0)^2 + q^2] \right\}. \quad (\text{B.8})$$

In order to check that this equation misses the  $s$ -channel contribution, as hinted by the lack of the corresponding crossing, we proceed to take the spectral functions in the bare, one-loop limit, i.e.  $\rho_T^{FG}(Q) \approx -2\text{Im}\Pi_R^T(Q)/Q^4$  and similarly for  $\rho_L^{FG}(Q)$ . In this way we can use the known form of the thermal polarisation tensor — see e.g. [36, 84] for the unintegrated Feynman-gauge expressions and [55, 85] for the analytical momentum integration yielding polylogarithms — to find, for space-like  $Q$

$$\text{Im}\Pi_R^L(Q) = \frac{g_3^2}{8\pi q^3} (q^2 - q_0^2) [N_c(-q^2 L_{1b} + 4qL_{2b} + 8L_{3b}) - 8T_F N_f (qL_{2f} + 2L_{3f})], \quad (\text{B.9})$$

$$\text{Im}\Pi_R^T(Q) = \frac{g_3^2}{4\pi q^3} (q^2 - q_0^2) [-N_c(q^2 L_{1b} + qL_{2b} + 2L_{3b}) + T_F N_f (q^2 L_{1f} + 2qL_{2f} + 4L_{3f})], \quad (\text{B.10})$$

where  $L_{nb} \equiv L_n$  with  $\tau_1 = \sigma_1 = 1$  and  $L_{nf} \equiv L_n$  with  $\tau_1 = \sigma_1 = -1$ , with  $L_n$  given in Eqs. (A.10)–(A.12). Upon plugging these expressions in Eq. (B.8) we obtain

$$\Gamma(k)_{\text{pc+cp}}^{[26]} = \frac{(N_c^2 - 1)g_3^6}{2^{13}\pi^7 k^2 f_{\text{PQ}}^2} \int_{-\infty}^k dq^0 \int_{|q_0|}^{2k-q^0} dq [1 + n_{\text{B}}(q^0) + n_{\text{B}}(k - q^0)] (q^2 - q_0^2) \times \left\{ N_c \left[ \frac{(3(q_0 - 2k)^2 - q^2) (q^2 L_{1b} + 6qL_{2b} + 12L_{3b})}{6q^4} + \frac{5}{3} L_{1b} \right] + 2T_F N_f \left[ \frac{(q^2 - 3(q_0 - 2k)^2) (q^2 L_{1f} + 6qL_{2f} + 12L_{3f})}{6q^4} - \frac{2}{3} L_{1f} \right] \right\}. \quad (\text{B.11})$$

Let us look back at Eq. (A.18). The  $t$ -channel and  $u$ -channel contribution thereto reads<sup>14</sup>

$$\Gamma(k)_{\text{KSVZ}}^{\text{strict LO } t+u} = \frac{g_3^6 (N_c^2 - 1)}{2^{13}\pi^7 f_{\text{PQ}}^2 k^2} \int_{-\infty}^k dq_0 \int_{|q_0|}^{2k-q_0} dq \left[ -N_c I_{+++}^t(1, 1) + 2T_F N_f I_{--+}^t(1, 0) - \frac{4\pi^2 T^3 k^2 (q^2 - q_0^2)}{q^4} (N_c + T_F N_f) \right] + \frac{g_3^4 (N_c^2 - 1) T m_{\text{D}}^2}{2^{10}\pi^5 f_{\text{PQ}}^2} \ln \left( \frac{4k^2}{m_{\text{D}}^2} \right), \quad (\text{B.13})$$

<sup>14</sup>This can be obtained by exploiting the definitions in Eqs. (A.6)–(A.7) and by noting that the proper separation of the  $gg \rightarrow ga$  matrix element squared into the three channels, as obtained by explicit computation of the diagrams in Feynman gauge as in [26], reads

$$|\mathcal{M}_{g+g \rightarrow g+a}|^2 = \frac{g_3^6 (N_c^2 - 1) N_c}{32\pi^4 f_{\text{PQ}}^2} \left[ \underbrace{\frac{su}{t}}_t - t + \underbrace{\frac{st}{u}}_u - u + \underbrace{\frac{tu}{s}}_s - s \right]. \quad (\text{B.12})$$

This is clearly equivalent to Eq. (B.12) and the  $t$ - and  $u$ -channel contributions come from the terms thus labeled.

Neglecting for a moment the subtraction of the IR-divergent part and its replacement by the analytical result in Eq. (2.16), we see that Eq. (B.11) agrees with Eq. (B.13), thus showing the lack of the  $s$ -channel contribution in the small  $g_3$  limit of the results of [26].<sup>15</sup>

What we have discussed is in our opinion not the main reason for which the method of [26] does not reproduce the strict LO result at small  $g_3$ . To explain why, we now need to turn to the IR sector of the cut-pole and pole-cut expression (B.6). For illustration purposes we keep using the bare spectral function for the transverse pole, leading to Eq. (B.8). Let us now inspect the soft intermediate-gluon sector: for  $q_0, q \sim g_3 T \ll k$ , we find

$$\Gamma(k)_{\text{pc+cp soft}}^{[26]} = \frac{(N_c^2 - 1)g_3^4}{2^{10}\pi^6 f_{\text{PQ}}^2} \int_{\mathcal{O}(g_3 T)} dq^0 dq q \frac{T}{q_0} (q^2 - q_0^2) \left[ \rho_L^{FG}(Q) + \rho_T^{FG}(Q) \left( 1 - \frac{q_0^2}{q^2} \right) \right]. \quad (\text{B.14})$$

Here  $\int_{\mathcal{O}(g_3 T)}$  means that this form of the integrand is valid for  $q_0, q \sim g_3 T$ . As we have explained in Sec. 2.2, the strict LO result emerges from using gauge-invariant HTL-resummed spectral functions. Are the Feynman-gauge expressions above equivalent to these in that limit at small  $g_3$ ? Naively, one would expect that to be the case, since HTLs are precisely the  $\mathcal{O}(g_3^2 T^2)$  gauge-invariant limit of thermal polarization tensors for soft external momenta. Indeed, Eq. (B.14) would agree with Eq. (2.11) if the soft- $Q$  Feynman-gauge spectral functions were to agree with the HTL ones.

There is however a subtlety related to the transverse spectral function, which in a generic space-like regime reads, following from Eq. (B.4)

$$\rho_T^{FG}(Q) = \frac{-2\text{Im} \Pi_R^T(Q)}{(Q^2 - \Pi_R^{\text{vac}}(Q) - \text{Re} \Pi_R^T(Q))^2 + (\text{Im} \Pi_R^T(Q))^2}. \quad (\text{B.15})$$

The subtlety is that, though parametrically  $\text{Re} \Pi_R^T(Q \sim g_3 T) = \text{Re} \Pi_R^{\text{HTL}}(Q) + \mathcal{O}(g_3^3 T^2)$ , there is a region where the real part of the transverse HTL self-energy vanishes and the subleading, gauge dependent term takes over. This happens when  $q_0 \rightarrow 0, q \lesssim g_3 T$ . In this region

$$\text{Im} \Pi_R^T(q_0 \rightarrow 0, q \lesssim g_3 T) = -\frac{\pi m_D^2 q^0}{4q} - \frac{g_3^2 N_c q^0 T}{4\pi} + \mathcal{O}(g_3^2 q_0^3 T^2 / q^2, g_3^2 q^0 q), \quad (\text{B.16})$$

where the first term on the r.h.s. is the HTL term and the second is its first correction. Hence  $\text{Im} \Pi_R^T(Q) \propto q^0$ , so that it vanishes at the denominator of Eq. (B.15), whereas at the numerator the power of  $q^0$  is absorbed by the  $T/q^0$  in Eq. (B.14), which stems from the classical-field tail of the Bose–Einstein distribution  $n_B(q^0)$ . The real part reads instead — see

---

<sup>15</sup>The  $s$ -channel part of the matrix elements and the corresponding diagrams appear in intermediate stages of the derivation of [26]. However, they are then subtracted, see Eq. (2.8) and Table 1 there. If the pole-pole contribution were to include a one-loop width, their method would account for them.

[52, 53] for the linear term in  $q$

$$\begin{aligned} \Pi_R^{\text{vac}}(0, q) + \text{Re} \Pi_R^T(0, q \ll T) = & -\frac{3g_3^2 N_c q T}{16} + \frac{g_3^2 q^2}{(4\pi)^2} \left( \frac{5}{3} N_c - \frac{4}{3} T_F N_f \right) \ln \frac{(4\pi T)^2}{e^{2\gamma_E} \bar{\mu}^2} \\ & + \frac{g_3^2 q^2}{3(4\pi)^2} \left[ \frac{28}{3} N_c + 4T_F N_f \left( 2 \ln 4 - \frac{5}{3} \right) \right] + \dots, \end{aligned} \quad (\text{B.17})$$

where  $\gamma_E$  is the Euler–Mascheroni constant. This expression shows clearly how in this region the HTL vanishes altogether: there is no  $g_3^2 T^2$  term. Furthermore, though we have kept only the first two terms of the  $q/T$  expansion, we find that the expression (B.17) describes well the full numerical expression even at  $q \approx 2T$ .

We are then at the crux of the problem: Eq. (B.17) is negative both in the numerical form and in the approximate one. When plugged in the spectral function in Eq. (B.15) it creates, together with the vanishing width at the denominator, a pole on the integration range. Let us keep for illustration the leading, linear term in Eq. (B.17) and plug it in Eq. (B.14): the divergent contribution is then

$$\Gamma(k)_{\text{pc+cp}}^{[26] \text{ div}} \approx \frac{(N_c^2 - 1) g_3^4 T m_D^2}{2^{11} \pi^5 f_{\text{PQ}}^2} \int_{\mathcal{O}(g_3^2 T)} dq \int_{-q_0^*}^{q_0^*} dq^0 \frac{1 + \mathcal{O}(q/T)}{\left( q - \frac{3}{16} g_3^2 N_c T \right)^2 + \pi^2 m_D^4 \frac{q_0^2}{16q^4}} \quad (\text{B.18})$$

$$= \frac{(N_c^2 - 1) g_3^4 T}{2^8 \pi^6 f_{\text{PQ}}^2} \int_{\mathcal{O}(g_3^2 T)} \frac{dq q^2}{q - \frac{3}{16} g_3^2 N_c T} \arctan \frac{q_0^* \pi m_D^2 / 4}{q^2 \left( q - \frac{3}{16} g_3^2 N_c T \right)} \quad (\text{B.19})$$

$$\approx \frac{9(N_c^2 - 1) N_c^2 g_3^8 T^3}{2^{17} \pi^5 f_{\text{PQ}}^2} \int_{\mathcal{O}(g_3^2 T)} \frac{dq}{\left| q - \frac{3}{16} g_3^2 N_c T \right|} \rightarrow \infty, \quad (\text{B.20})$$

where for illustration we replaced only the HTL term of Eq. (B.16) in Eq. (B.15).  $g_3^4 T \ll q_0^* \ll g_3^2 T$  is a cutoff that singles out the divergent region where these approximations are valid.

Eqs. (B.18)–(B.20) then show how the gauge-dependent resummation of [26, 36], even when taken at small  $g_3$ , results in a divergent contribution. We have checked numerically that this divergence persists when the full form of the HTL time-like spectral functions and of the Feynman-gauge resummed spectral function (B.15) are used, both for  $g_3 \ll 1$  and  $g_3 \gtrsim 1$ . It is not clear to us how this divergence was regulated in the numerical results of [26], but we believe it to be the main source of the  $\mathcal{O}(10)$  discrepancy between our results and theirs for  $F_3$  discussed in and around Fig. 6. We can speculate that, if the analytical expressions (B.9)–(B.10) for the imaginary parts of the self-energies are replaced by interpolators, these might generate a nonvanishing  $\text{Im} \Pi_R^T(0, q)$ . This would in turn artificially regulate Eq. (B.20) and inflate the result obtained from this method when compared to the ones we present in the main text.<sup>16</sup>

<sup>16</sup> Let us assume for argument’s sake that this interpolating procedure introduces a minimum value  $\gamma_{\text{num}}^2 > 0$  for  $(\text{Im} \Pi_R^T(q^0 \rightarrow 0, q))^2$ . Then the spectral-function denominator in Eq. (B.18) turns into  $(q - 3g_3^2 N_c T / 16)^2 + \min(\pi^2 m_D^4 q_0^2 / (16q^2), \gamma_{\text{num}}^2) / q^2$ . Let us assume that the switchover between the proper, odd imaginary part and the artificial numerical width  $\gamma_{\text{num}}$  happens for frequencies  $\tilde{q}^0 = \pm 4\gamma_{\text{num}} q / (\pi m_D^2)$  obeying  $\tilde{q}_0^2 < q_0^{*2}$ . Then,

Let us note that this divergence is gauge-dependent and known. As found in the early eighties in [52, 53] and illustrated in the textbook [84], the position of the pole at  $q \approx 3g_3^2 N_c T/16$  shifts in a generic covariant gauge to  $q \approx [8 + (\xi + 1)^2]g_3^2 N_c T/64 > 0$  for all  $\xi$ , with  $\xi$  the gauge parameter,  $\xi = 1$  for Feynman gauge. Physically, this pole would be absent for an abelian theory: it occurs for  $q \sim g_3^2 T$  and arises from self-interactions of soft, transverse gluons, hence the proportionality to  $N_c$ . As pointed out long ago in [52, 53, 86] and summarized in [84], this means that this gauge-dependent resummation has introduced an artificial sensitivity to this ultrasoft, chromomagnetic scale where perturbation theory breaks down [54]. We recall that, as we mentioned in the main text, [55] analyzed an altogether similar problem for transverse momentum broadening and reached the same conclusions we are drawing here. To avoid this spurious pole, they introduced a scheme that resums the HTL self-energy for  $Q \lesssim g_3 T$  and the full one above. Indeed, if one drops the non-HTL  $-3/16g_3^2 N_c T$  term from the denominator in Eq. (B.18), one recovers the IR-finite, pathology-free HTL contribution in this region.

For these reasons, we think that this pathology of the gauge-dependent resummation scheme is not unique to axion production — gravitino [36] and axino [81] calculations would also be affected. See also [87, 88] for recent improvements on the gravitino calculations that do not, however, seem to touch the main issue of the divergence.

restricting ourselves to the frequency range  $q_0^2 < \tilde{q}_0^2$ , this numerically-regulated result differs from Eqs. (B.18)–(B.20). It reads

$$\begin{aligned} \Gamma(k)_{\text{pc+cp}}^{[26] \text{ div num}} &= \frac{(N_c^2 - 1)g_3^4 T m_D^2}{2^{11} \pi^5 f_{\text{PQ}}^2} \int_{\mathcal{O}(g_3^2 T)} dq \int_{-\tilde{q}_0}^{\tilde{q}_0} dq^0 \frac{q^2}{(q^2 - \frac{3}{16}g_3^2 N_c T q)^2 + \gamma_{\text{num}}^2} \\ &= \frac{(N_c^2 - 1)g_3^4 T \gamma_{\text{num}}}{2^8 \pi^6 f_{\text{PQ}}^2} \int_{\mathcal{O}(g_3^2 T)} \frac{dq q^3}{(q^2 - \frac{3}{16}g_3^2 N_c T q)^2 + \gamma_{\text{num}}^2} \approx \frac{9(N_c^2 - 1)N_c^2 g_3^8 T^3}{2^{16} \pi^5 f_{\text{PQ}}^2} \left[ 1 + \mathcal{O}\left(\frac{\gamma_{\text{num}}}{g_3^4 T^2}\right) \right], \end{aligned} \quad (\text{B.21})$$

where we performed the  $q$  integration over the pole region, exploiting its Lorentzian-like shape. This artificially regulated quantity is finite, unlike Eq. (B.20). We remark that we have introduced a numerical width  $\gamma_{\text{num}}$  only in the denominator of Eq. (B.15). Were we to assume the same for the numerator, we would need to multiply the r.h.s. on the first line of Eq. (B.21) by  $\gamma_{\text{num}}/(\pi m_D^2 q^0/(4q))$ , which would give a vanishing contribution if the  $dq^0/q^0$  integration is treated as a principal value.

Let us further note that in Eq. (B.21) we only considered the contribution from  $0 < q_0^2 < \tilde{q}_0^2$ , which is where the divergence shows up in the absence of numerical regularization. The range  $q_0^{*2} > q_0^2 > \tilde{q}_0^2$  depends then much more strongly on  $\gamma_{\text{num}}$  — logarithmically, in fact — than Eq. (B.21), i.e.

$$\begin{aligned} \Gamma(k)_{\text{pc+cp}}^{[26] \text{ div num remainder}} &= \frac{(N_c^2 - 1)g_3^4 T m_D^2}{2^{11} \pi^5 f_{\text{PQ}}^2} \int_{\mathcal{O}(g_3^2 T)} dq \int_{\tilde{q}_0}^{q_0^*} dq^0 \frac{2}{(q - \frac{3}{16}g_3^2 N_c T)^2 + \pi^2 m_D^4 \frac{q_0^2}{16q^4}} \\ &= \frac{(N_c^2 - 1)g_3^4 T}{2^8 \pi^6 f_{\text{PQ}}^2} \int_{\mathcal{O}(g_3^2 T)} \frac{dq q^2}{q - \frac{3}{16}g_3^2 N_c T} \left[ \arctan\left(\frac{q_0^* \pi m_D^2/4}{q^2 (q - \frac{3}{16}g_3^2 N_c T)}\right) - \arctan\left(\frac{\gamma_{\text{num}}}{q (q - \frac{3}{16}g_3^2 N_c T)}\right) \right] \\ &\approx \frac{9(N_c^2 - 1)N_c^2 g_3^8 T^3}{2^{16} \pi^5 f_{\text{PQ}}^2} \ln \frac{4q_0^* \pi m_D^2}{3g_3^2 N_c T \gamma_{\text{num}}}. \end{aligned} \quad (\text{B.22})$$

It is this logarithmic dependence on the regulator that would be responsible, under this hypothesis, for an unphysical upward shift of the rate.



We conclude with two final remarks. First, the authors of [26, 36] justify their scheme by noting that the HTL spectral function is a good approximation to the full one-loop one only for  $Q \ll T$  and should thus not be used for all  $Q$ . We agree with this only partially. Let us look at the spectral function of a resummed propagator in the cut regime, such as the one given by Eq. (B.15). It features the imaginary part of the self-energy at the numerator, whereas the denominator contains both the real and the imaginary parts. Crucially, it is only the (imaginary part of the) self-energy at the numerator that must do away with the HTL approximation, so that it can be used for all  $Q$ . The denominator can instead be kept in the HTL approximation, as self-energy resummation is only relevant at soft  $Q$ , where the HTL holds. Indeed, this corresponds precisely to the scheme of [59, 60], of which our tuned mass scheme is a simplified implementation. As the previous discussion has shown, replacing HTL self-energies at the denominator with full, gauge-dependent ones leads to well-known pathologies in non-abelian gauge theories.

Finally, this gauge-dependent resummation scheme would not be pathological for abelian gauge theories, where the one-loop gauge-boson self-energy is actually gauge invariant. Provided the problem with the  $s$ -channel contribution is addressed, the method of [26, 36] would then provide another scheme that agrees with the strict one at small  $g_1$ . By the arguments of this section and of App. A — see in particular Eqs. (A.25) and Eq. (A.26) and the text around them — we expect that this scheme would differ from the strict one at relative  $\mathcal{O}(g_1)$  for a theory with light bosonic (and possibly fermionic) charge carriers, such as the  $U(1)$  component of the SM in the symmetric phase. For a QED-like theory with fermionic charge carriers only, the difference would be  $\mathcal{O}(g_1^2)$ .<sup>17</sup> Hence, we do not think that this abelian, amended version of the method of [26, 36] would be an any more natural extrapolation to the  $g_1 \sim 1$  range than our tuned scheme, which is, we remark, far lighter from a numerical standpoint.

## C Theory uncertainty in perturbative thermal QCD

The calculation of the thermal axion rate in the KSVZ model is essentially a perturbative calculation in hot QCD. In particular, the temperature range where the reliability of such a calculation is most uncertain is in the vicinity of the QCD transition. To this end, we summarize here a few important findings from the hot QCD and heavy-ion collision literature that are directly relevant to our case. We refer to [58] for a comprehensive review of perturbative hot QCD.

As mentioned, the axion rate is strongly connected with the transverse momentum broadening coefficient  $\hat{q}$ . Indeed, they are both part of a broader class of *dynamical observables*,

---

<sup>17</sup>Recently, [89] determined the shear viscosity of hot and dense QCD at leading- and next-to-leading order. For baryon chemical potentials sufficiently larger than the temperature, the one-loop gluon self-energy is dominated by the gauge-invariant quark loop. The authors thus compared the numerical impact of resumming HTL and full self-energies in the denominators. In this well-defined and pathology-free case they find that the discrepancy is  $\mathcal{O}(10\%)$  or less at intermediate couplings, in full agreement with our argument here.

to be opposed to *thermodynamical ones*. The latter, such as the pressure, energy density, entropy, etc., are given by thermal expectation values of local operators, e.g. the energy-momentum tensor. The former, on the other hand, are given by operators that are non-local in time, such as the retarded two-point function giving the axion rate in Eqs. (2.9) and (2.10).

This important distinction makes it so that thermodynamical observables can readily be evaluated in compactified Euclidean spacetime. They are amenable (at vanishing baryon chemical potential) to precise lattice determinations and to high-order perturbative ones. As summarised e.g. in [58], perturbative determinations of the pressure through sophisticated resummations and Effective Field Theories reach N<sup>4</sup>LO and are in reasonable agreement, though with large uncertainties, with lattice QCD at temperatures above twice the pseudo-critical one. These perturbative determinations also show the role that physics at or below the soft  $g_3 T$  scale plays in the apparent slow convergence of the expansion. It bears repeating that no gauge-dependent resummations of the full one-loop gluon self-energies are performed in these calculations, as the community is aware of the pathologies that arise, as discussed in the previous appendix.

For what concerns dynamical quantities, much less is known. Direct lattice determinations are not possible, as these quantities are intrinsically Minkowskian and require a highly non-trivial analytical continuation from Euclidean space-time, in the form of an ill-posed inverse problem — see e.g. [90] for a review. Perturbative determinations too are more challenging, with most quantities being known to leading order. NLO corrections, of relative  $\mathcal{O}(g_3)$ , have been determined only for a handful of observables, as reviewed by one of us in [58]. These include the momentum broadening coefficient of heavy quarks in [62, 63], that of light quarks and gluon —  $\hat{q}$  — in [57], the photon production rate in [48], the shear viscosity in [65] and the isotropic thermalisation time in [64].

As summarised briefly in [72], observables that are directly sensitive to the physics of transverse momentum broadening, such as  $\hat{q}$  itself and the shear viscosity, show large  $\mathcal{O}(g_3)$  corrections, which overtake the LO at  $g_3 \sim 0.5$ . On the other hand, processes that are not directly sensitive to that physics, such as photon production and isotropic thermalisation, have  $\mathcal{O}(g_3)$  corrections at the 30% level even when extrapolating to  $\alpha_s \sim 0.3$  ( $g_3 \sim 2$ ) which is the expected value in the vicinity of the QCD crossover. As we mentioned, one possible explanation could lie in an “overscreening” in the leading-order formulation of transverse momentum broadening [71].

We further remark that the NLO calculation of the shear viscosity in [65] included many different  $\mathcal{O}(g_3)$  contributions, coming from several different momentum regions and physical mechanisms. One of the main findings was that NLO corrections to  $\hat{q}$  dwarf all others. This motivates our NLO Ansatz as a proxy for conservatively “very large” NLO contributions and further suggests how important transverse-momentum-broadening physics might not be captured in the “overscreened” LO formulation of  $\hat{q}$ . We also mention that non-perturbative, all-orders determinations of the soft, classical contribution to transverse momentum broadening in [73, 74, 91, 92] through dimensionally-reduced lattice field theory point to a smaller value for  $\hat{q}$  than that obtained at NLO.

Finally, we remark that our methodology of comparing several LO-equivalent determinations of a dynamical quantity is well rooted in the hot QCD literature. For instance, when computing the shear viscosity and quark number diffusion to leading order, the authors of [60] compared results obtained by resumming HTL self-energies in the naively divergent denominators with other LO-equivalent schemes where HTL resummation is switched off above an exchanged three- or four-momentum of the order of the temperature — see Fig. 4 there, finding an  $\mathcal{O}(1)$  uncertainty for  $m_D/T \approx 2$ . [62, 63] compared strict and tuned-like LO schemes with their new NLO determination of heavy-quark momentum broadening. More recently, [93] compared results for non-equilibrium dynamics from the QCD kinetic theory obtained from their implementation of a tuned scheme and from the HTL-resummed denominator, as per [59]. In particular, their Sec. V.G and Fig. 10 explicitly consider the case of  $\hat{q}$ , finding a small discrepancy between the two.

## References

- [1] R.D. Peccei and H.R. Quinn, *Constraints Imposed by CP Conservation in the Presence of Instantons*, *Phys. Rev. D* **16** (1977) 1791.
- [2] S. Weinberg, *A New Light Boson?*, *Phys. Rev. Lett.* **40** (1978) 223.
- [3] F. Wilczek, *Problem of Strong P and T Invariance in the Presence of Instantons*, *Phys. Rev. Lett.* **40** (1978) 279.
- [4] J. Preskill, M.B. Wise and F. Wilczek, *Cosmology of the Invisible Axion*, *Phys. Lett. B* **120** (1983) 127.
- [5] L.F. Abbott and P. Sikivie, *A Cosmological Bound on the Invisible Axion*, *Phys. Lett. B* **120** (1983) 133.
- [6] M. Dine and W. Fischler, *The Not So Harmless Axion*, *Phys. Lett. B* **120** (1983) 137.
- [7] D.J.E. Marsh, *Axion Cosmology*, *Phys. Rept.* **643** (2016) 1 [[1510.07633](#)].
- [8] L. Di Luzio, M. Giannotti, E. Nardi and L. Visinelli, *The landscape of QCD axion models*, *Phys. Rept.* **870** (2020) 1 [[2003.01100](#)].
- [9] PLANCK collaboration, *Planck 2018 results. VI. Cosmological parameters*, *Astron. Astrophys.* **641** (2020) A6 [[1807.06209](#)].
- [10] T.-H. Yeh, J. Shelton, K.A. Olive and B.D. Fields, *Probing physics beyond the standard model: limits from BBN and the CMB independently and combined*, *JCAP* **10** (2022) 046 [[2207.13133](#)].
- [11] CMB-S4 collaboration, *CMB-S4 Science Book, First Edition*, [1610.02743](#).
- [12] K. Abazajian et al., *CMB-S4 Science Case, Reference Design, and Project Plan*, [1907.04473](#).
- [13] CMB-S4 collaboration, *Snowmass 2021 CMB-S4 White Paper*, [2203.08024](#).
- [14] J.J. Bennett, G. Buldgen, M. Drewes and Y.Y.Y. Wong, *Towards a precision calculation of the effective number of neutrinos  $N_{\text{eff}}$  in the Standard Model I: the QED equation of state*, *JCAP* **03** (2020) 003 [[1911.04504](#)].

- [15] J.J. Bennett, G. Buldgen, P.F. De Salas, M. Drewes, S. Gariazzo, S. Pastor et al., *Towards a precision calculation of  $N_{\text{eff}}$  in the Standard Model II: Neutrino decoupling in the presence of flavour oscillations and finite-temperature QED*, *JCAP* **04** (2021) 073 [[2012.02726](#)].
- [16] M. Cielo, M. Escudero, G. Mangano and O. Pisanti, *Neff in the Standard Model at NLO is 3.043*, *Phys. Rev. D* **108** (2023) L121301 [[2306.05460](#)].
- [17] M. Drewes, Y. Georis, M. Klasen, L.P. Wiggering and Y.Y.Y. Wong, *Towards a precision calculation of  $N_{\text{eff}}$  in the Standard Model. Part III. Improved estimate of NLO contributions to the collision integral*, *JCAP* **06** (2024) 032 [[2402.18481](#)].
- [18] A. Notari, F. Rompineve and G. Villadoro, *Improved Hot Dark Matter Bound on the QCD Axion*, *Phys. Rev. Lett.* **131** (2023) 011004 [[2211.03799](#)].
- [19] F. Bianchini, G.G. di Cortona and M. Valli, *The QCD Axion: Some Like It Hot*, [2310.08169](#).
- [20] F. D’Eramo, F. Hajkarim and A. Lenoci, *Dark radiation from the primordial thermal bath in momentum space*, *JCAP* **03** (2024) 009 [[2311.04974](#)].
- [21] J.E. Kim, *Weak Interaction Singlet and Strong CP Invariance*, *Phys. Rev. Lett.* **43** (1979) 103.
- [22] M.A. Shifman, A.I. Vainshtein and V.I. Zakharov, *Can Confinement Ensure Natural CP Invariance of Strong Interactions?*, *Nucl. Phys. B* **166** (1980) 493.
- [23] E. Braaten and T.C. Yuan, *Calculation of screening in a hot plasma*, *Phys. Rev. Lett.* **66** (1991) 2183.
- [24] E. Masso, F. Rota and G. Zsembinszki, *On axion thermalization in the early universe*, *Phys. Rev. D* **66** (2002) 023004 [[hep-ph/0203221](#)].
- [25] P. Graf and F.D. Steffen, *Thermal axion production in the primordial quark-gluon plasma*, *Phys. Rev. D* **83** (2011) 075011 [[1008.4528](#)].
- [26] A. Salvio, A. Strumia and W. Xue, *Thermal axion production*, *JCAP* **01** (2014) 011 [[1310.6982](#)].
- [27] F. D’Eramo, F. Hajkarim and S. Yun, *Thermal Axion Production at Low Temperatures: A Smooth Treatment of the QCD Phase Transition*, *Phys. Rev. Lett.* **128** (2022) 152001 [[2108.04259](#)].
- [28] F. D’Eramo, F. Hajkarim and S. Yun, *Thermal QCD Axions across Thresholds*, *JHEP* **10** (2021) 224 [[2108.05371](#)].
- [29] F. D’Eramo, E. Di Valentino, W. Giarè, F. Hajkarim, A. Melchiorri, O. Mena et al., *Cosmological bound on the QCD axion mass, redux*, *JCAP* **09** (2022) 022 [[2205.07849](#)].
- [30] E. Braaten and R.D. Pisarski, *Soft Amplitudes in Hot Gauge Theories: A General Analysis*, *Nucl.Phys.* **B337** (1990) 569.
- [31] E. Braaten and R.D. Pisarski, *Simple effective Lagrangian for hard thermal loops*, *Phys. Rev.* **D45** (1992) 1827.
- [32] D. Besak and D. Bodeker, *Thermal production of ultrarelativistic right-handed neutrinos: Complete leading-order results*, *JCAP* **03** (2012) 029 [[1202.1288](#)].
- [33] J. Ghiglieri and M. Laine, *Neutrino dynamics below the electroweak crossover*, *JCAP* **1607** (2016) 015 [[1605.07720](#)].

- [34] J. Ghiglieri, G. Jackson, M. Laine and Y. Zhu, *Gravitational wave background from Standard Model physics: Complete leading order*, *JHEP* **07** (2020) 092 [[2004.11392](#)].
- [35] M.C.A. York, A. Kurkela, E. Lu and G.D. Moore, *UV Cascade in Classical Yang-Mills via Kinetic Theory*, *Phys.Rev.* **D89** (2014) 074036 [[1401.3751](#)].
- [36] V.S. Rychkov and A. Strumia, *Thermal production of gravitinos*, *Phys. Rev. D* **75** (2007) 075011 [[hep-ph/0701104](#)].
- [37] M. Becker, E. Copello, J. Harz and C. Tamarit, *Dark matter freeze-in from non-equilibrium QFT: towards a consistent treatment of thermal effects*, [2312.17246](#).
- [38] A. Alloul, N.D. Christensen, C. Degrande, C. Duhr and B. Fuks, *FeynRules 2.0 - A complete toolbox for tree-level phenomenology*, *Comput. Phys. Commun.* **185** (2014) 2250 [[1310.1921](#)].
- [39] T. Hahn, *Generating Feynman diagrams and amplitudes with FeynArts 3*, *Comput. Phys. Commun.* **140** (2001) 418 [[hep-ph/0012260](#)].
- [40] T. Hahn, S. Paßehr and C. Schappacher, *FormCalc 9 and Extensions*, *PoS* **LL2016** (2016) 068 [[1604.04611](#)].
- [41] V. Klimov, *Spectrum of Elementary Fermi Excitations in Quark Gluon Plasma. (In Russian)*, *Sov. J. Nucl. Phys.* **33** (1981) 934.
- [42] V. Klimov, *Collective Excitations in a Hot Quark Gluon Plasma*, *Sov. Phys. JETP* **55** (1982) 199.
- [43] H. Weldon, *Effective Fermion Masses of Order  $gT$  in High Temperature Gauge Theories with Exact Chiral Invariance*, *Phys. Rev. D* **26** (1982) 2789.
- [44] H.A. Weldon, *Covariant Calculations at Finite Temperature: The Relativistic Plasma*, *Phys. Rev. D* **26** (1982) 1394.
- [45] G. Baym, H. Monien, C.J. Pethick and D.G. Ravenhall, *Transverse Interactions and Transport in Relativistic Quark - Gluon and Electromagnetic Plasmas*, *Phys. Rev. Lett.* **64** (1990) 1867.
- [46] P.B. Arnold, G.D. Moore and L.G. Yaffe, *Photon emission from ultrarelativistic plasmas*, *JHEP* **0111** (2001) 057 [[hep-ph/0109064](#)].
- [47] P.B. Arnold, G.D. Moore and L.G. Yaffe, *Photon emission from quark gluon plasma: Complete leading order results*, *JHEP* **0112** (2001) 009 [[hep-ph/0111107](#)].
- [48] J. Ghiglieri, J. Hong, A. Kurkela, E. Lu, G.D. Moore and D. Teaney, *Next-to-leading order thermal photon production in a weakly coupled quark-gluon plasma*, *JHEP* **1305** (2013) 010 [[1302.5970](#)].
- [49] D. Bödeker, M. Sangel and M. Wörmann, *Equilibration, particle production, and self-energy*, *Phys. Rev. D* **93** (2016) 045028 [[1510.06742](#)].
- [50] J. Ghiglieri and D. Teaney, *Parton energy loss and momentum broadening at NLO in high temperature QCD plasmas*, *Int. J. Mod. Phys.* **E24** (2015) 1530013 [[1502.03730](#)].
- [51] A. Brandenburg and F.D. Steffen, *Axino dark matter from thermal production*, *JCAP* **08** (2004) 008 [[hep-ph/0405158](#)].
- [52] O.K. Kalashnikov and V.V. Klimov, *INFRARED BEHAVIOR OF GREEN FUNCTIONS IN YANG-MILLS THEORY AT FINITE TEMPERATURES*, *Yad. Fiz.* **33** (1980) 848.

- [53] K. Kajantie and J.I. Kapusta, *Behavior of Gluons at High Temperature*, *Annals Phys.* **160** (1985) 477.
- [54] A.D. Linde, *Infrared Problem in Thermodynamics of the Yang-Mills Gas*, *Phys.Lett.* **B96** (1980) 289.
- [55] F. D’Eramo, M. Lekaveckas, H. Liu and K. Rajagopal, *Momentum Broadening in Weakly Coupled Quark-Gluon Plasma (with a view to finding the quasiparticles within liquid quark-gluon plasma)*, *JHEP* **05** (2013) 031 [[1211.1922](#)].
- [56] P. Aurenche, F. Gelis and H. Zaraket, *A Simple sum rule for the thermal gluon spectral function and applications*, *JHEP* **0205** (2002) 043 [[hep-ph/0204146](#)].
- [57] S. Caron-Huot,  *$O(g)$  plasma effects in jet quenching*, *Phys.Rev.* **D79** (2009) 065039 [[0811.1603](#)].
- [58] J. Ghiglieri, A. Kurkela, M. Strickland and A. Vuorinen, *Perturbative Thermal QCD: Formalism and Applications*, *Phys. Rept.* **880** (2020) 1 [[2002.10188](#)].
- [59] P.B. Arnold, G.D. Moore and L.G. Yaffe, *Effective kinetic theory for high temperature gauge theories*, *JHEP* **01** (2003) 030 [[hep-ph/0209353](#)].
- [60] P.B. Arnold, G.D. Moore and L.G. Yaffe, *Transport coefficients in high temperature gauge theories. 2. Beyond leading log*, *JHEP* **05** (2003) 051 [[hep-ph/0302165](#)].
- [61] K. Boguslavski, A. Kurkela, T. Lappi, F. Lindenbauer and J. Peuron, *Jet quenching parameter in QCD kinetic theory*, *Phys. Rev. D* **110** (2024) 034019 [[2312.00447](#)].
- [62] S. Caron-Huot and G.D. Moore, *Heavy quark diffusion in perturbative QCD at next-to-leading order*, *Phys.Rev.Lett.* **100** (2008) 052301 [[0708.4232](#)].
- [63] S. Caron-Huot and G.D. Moore, *Heavy quark diffusion in QCD and  $N=4$  SYM at next-to-leading order*, *JHEP* **02** (2008) 081 [[0801.2173](#)].
- [64] Y. Fu, J. Ghiglieri, S. Iqbal and A. Kurkela, *Thermalization of non-Abelian gauge theories at next-to-leading order*, *Phys. Rev. D* **105** (2022) 054031 [[2110.01540](#)].
- [65] J. Ghiglieri, G.D. Moore and D. Teaney, *QCD Shear Viscosity at (almost) NLO*, *JHEP* **03** (2018) 179 [[1802.09535](#)].
- [66] L.D. McLerran, E. Mottola and M.E. Shaposhnikov, *Sphalerons and Axion Dynamics in High Temperature QCD*, *Phys. Rev. D* **43** (1991) 2027.
- [67] M. Laine, L. Niemi, S. Procacci and K. Rummukainen, *Shape of the hot topological charge density spectral function*, *JHEP* **11** (2022) 126 [[2209.13804](#)].
- [68] M. Laine, P. Schicho and Y. Schröder, *A QCD Debye mass in a broad temperature range*, *Phys. Rev. D* **101** (2020) 023532 [[1911.09123](#)].
- [69] M. Laine and M. Meyer, *Standard Model thermodynamics across the electroweak crossover*, *JCAP* **07** (2015) 035 [[1503.04935](#)].
- [70] K. Bouzoud and J. Ghiglieri, *Dataset for the paper "Thermal axion production at hard and soft momenta"*, Zenodo (Apr., 2024), [10.5281/zenodo.10926565](#).
- [71] B. Müller,  *$\eta/s\hat{q}/T^3$  relation at next-to-leading order in QCD*, *Phys. Rev. D* **104** (2021) L071501 [[2107.14775](#)].

- [72] J. Ghiglieri, *Transport Properties of the QCD Medium*, *Acta Phys. Polon. Supp.* **16** (2023) 1 [[2207.11112](#)].
- [73] M. Panero, K. Rummukainen and A. Schäfer, *Lattice Study of the Jet Quenching Parameter*, *Phys. Rev. Lett.* **112** (2014) 162001 [[1307.5850](#)].
- [74] G.D. Moore and N. Schlusser, *Transverse momentum broadening from the lattice*, *Phys. Rev. D* **101** (2020) 014505 [[1911.13127](#)].
- [75] P. Gondolo and G. Gelmini, *Cosmic abundances of stable particles: Improved analysis*, *Nucl. Phys. B* **360** (1991) 145.
- [76] P. Carena, T. Fischer, M. Giannotti, G. Guo, G. Martínez-Pinedo and A. Mirizzi, *Improved axion emissivity from a supernova via nucleon-nucleon bremsstrahlung*, *JCAP* **10** (2019) 016 [[1906.11844](#)].
- [77] A. Caputo and G. Raffelt, *Astrophysical Axion Bounds: The 2024 Edition*, in *1st Training School of the COST Action COSMIC WISPerS (CA21106)*, 1, 2024 [[2401.13728](#)].
- [78] S. Weinberg, *Phenomenological Lagrangians*, *Physica A* **96** (1979) 327.
- [79] J. Gasser and H. Leutwyler, *Chiral Perturbation Theory to One Loop*, *Annals Phys.* **158** (1984) 142.
- [80] J. Gasser and H. Leutwyler, *Chiral Perturbation Theory: Expansions in the Mass of the Strange Quark*, *Nucl. Phys. B* **250** (1985) 465.
- [81] A. Strumia, *Thermal production of axino Dark Matter*, *JHEP* **06** (2010) 036 [[1003.5847](#)].
- [82] M.C. Galassi, J. Davies, J. Theiler, B. Gough, G. Jungman, P. Alken et al., *GNU Scientific Library*, Network Theory, Ltd. (8, 2019).
- [83] A. Voigt, *Polylogarithm*, Zenodo (Aug., 2022), [10.5281/zenodo.6951307](#).
- [84] J.I. Kapusta and C. Gale, *Finite-temperature field theory: Principles and applications*, Cambridge Monographs on Mathematical Physics, Cambridge University Press (2011), [10.1017/CBO9780511535130](#).
- [85] M. Laine, *NLO thermal dilepton rate at non-zero momentum*, *JHEP* **11** (2013) 120 [[1310.0164](#)].
- [86] U.W. Heinz, K. Kajantie and T. Toimela, *Gauge Covariant Linear Response Analysis of QCD Plasma Oscillations*, *Annals Phys.* **176** (1987) 218.
- [87] H. Eberl, I.D. Gialamas and V.C. Spanos, *Gravitino thermal production revisited*, *Phys. Rev. D* **103** (2021) 075025 [[2010.14621](#)].
- [88] H. Eberl, I.D. Gialamas and V.C. Spanos, *Gravitino Thermal Production, Dark Matter, and Reheating of the Universe*, [2408.16043](#).
- [89] I. Danhoni and G.D. Moore, *Hot and dense QCD shear viscosity at (almost) NLO*, *JHEP* **09** (2024) 075 [[2408.00524](#)].
- [90] H.B. Meyer, *Transport Properties of the Quark-Gluon Plasma: A Lattice QCD Perspective*, *Eur. Phys. J. A* **47** (2011) 86 [[1104.3708](#)].

- [91] G.D. Moore, S. Schlichting, N. Schlusser and I. Soudi, *Non-perturbative determination of collisional broadening and medium induced radiation in QCD plasmas*, *JHEP* **10** (2021) 059 [[2105.01679](#)].
- [92] S. Schlichting and I. Soudi, *Splitting rates in QCD plasmas from a nonperturbative determination of the momentum broadening kernel  $C(q_\perp)$* , *Phys. Rev. D* **105** (2022) 076002 [[2111.13731](#)].
- [93] K. Boguslavski and F. Lindenbauer, *Soft-gluon exchange matters: Isotropic screening in QCD kinetic theory*, *Phys. Rev. D* **110** (2024) 074017 [[2407.09605](#)].